Advances in Nano Research, *Vol. 19, No. 4 (2025) 319-333*
https://doi.org/10.12989/anr.2025.19.4.319

Nonlinear vibration induced by temperature in cylindrical sandwich microshells: An analytical investigation of size dependence in functionally graded graphene platelets reinforcement

M. Soltani Tehrani[1], M. Ruzieva[2], M. Djumaniyazova[3], G. Masharipova[4] and L. Nanji[*5]

[1]*Department of Civil Engineering, Najafabad Branch, Islamic Azad University, Najafabad, Iran*
[2]*Department of sport and psychology Mamun university Khiva Uzbekistan, 0009-0006-8541-1037*
[3]*Department of Pedagogy and Psychology Urgench state university Urgench, Uzbekistan, 0009-0008-8561-5720*
[4]*Department of social science Alfraganus University, Tashkent, Uzbekistan, 0009-0007-0788-2359*
[5]*Department of Engineering, Islamic Azad University of Khorramabad, Khorramabad, Iran*

(*Received February 25, 2022, Revised August 25, 2025, Accepted September 1, 2025*)

Abstract. Using the modified couple stress theory, this study investigates the nonlinear vibrations of a sandwich microshell composed of a functionally graded graphene platelets (FG-GPL)-reinforced core and two uniform outer skins, all simply supported. The analysis employs the first-order shear deformation shell theory alongside a nonlinear strain framework. The mechanical properties of the GPL-reinforced core are assumed to vary with thickness, utilizing the Halpin-Tsai model. Three distinct distribution patterns of GPLs throughout the thickness are examined. The microshell is subjected to thermal loading, facilitating the calculation of its temperature field across the thickness by applying the one-dimensional Fourier heat conduction equation, which accounts for thermal boundary conditions at both the inner and outer surfaces of the shell. The shell models incorporate shear deformation and rotary inertia, while geometric nonlinearity is addressed using the von Karman approach. The fundamental partial differential equations (PDEs) governing the system are derived using Hamilton's principle. These coupled PDEs are then transformed into a set of ordinary differential equations (ODEs) via the Galerkin method and solved using the multiple timescale method to obtain results. The findings are validated against existing literature, demonstrating a robust level of agreement. This study thoroughly examines the effects of various factors, including GPL weight fraction, thickness distribution patterns, material length scale parameters, core length, radius, and individual layer thickness on nonlinear frequency ratios, fundamental linear frequencies, and nonlinear frequencies.

Keywords: functionally graded graphene platelets; nonlinear vibration; sandwich shells; size dependent; thermal influence

1. Introduction

In contemporary times, the rapid advancement of technology in micro-scale structures necessitates the precise design of microstructures that accurately account for small-scale effects. Consequently, the modeling and analysis of size-dependent vibrational behaviors of microstructures are essential for achieving optimal designs. Furthermore, carbon-based materials, such as carbon nanotubes (CNTs) and graphene nanoplatelets (GPLs), which possess superior properties, have been utilized as nanofillers to create composite materials with exceptional characteristics. GPLs have been selected as the reinforcement phase in composites to manifest enhanced effects due to their elevated Young's modulus, rigidity, remarkable tensile strength, and outstanding thermal properties.

For instance, novel GPL-reinforced polymers exhibit significant potential for application across various technologies and engineering domains. In recent years, numerous investigations by researchers have concentrated on the mechanical and vibrational behaviors of GPL-reinforced composites (Huang *et al*. 2012, Kim *et al*. 2010).

This discussion will provide a brief overview of current analyses concerning FG and sandwich structures, particularly those composed of functionally graded GPL-reinforced composites. Utilizing the differential quadrature method (DQM), the free vibration analysis of functionally graded curved thick panels under various boundary conditions was explored by Zahedinejad *et al*. (2010) based on three-dimensional elasticity theory. Jafari *et al*. (2014) reported on the nonlinear vibration analysis of simply supported functionally graded cylindrical shells with piezoelectric layers, employing the nonlinear Donnell's theory. Hosseini-Hashmi *et al*. (2015) conducted frequency analysis of functionally graded panels made of polymeric foam under Levy-type boundary conditions, utilizing first-order shear deformation theory (FSDT) in conjunction with Sanders' theory based on a state-space method. The free vibration analysis of fiber-reinforced cylindrical panels was performed using a three-dimensional mesh-free model at various boundary conditions by Soltani maleki *et al*. (2016). Shen *et al*. (2017) investigated the nonlinear vibrational behavior of GPL-reinforced composite shells in a thermal medium based on third-order shear deformation theory (TSDT) and von Kármán-type relations. Dong *et al*. (2018) provided an

*Corresponding author, M.Sc.,
E-mail: leila.iranshahi2023@gmail.com

ISSN: 2287-237X (Print), 2287-2388 (Online)

analytical solution for the free vibration assessment of rotating GPL-reinforced cylindrical shells. Niu *et al*. (2019) developed the Chebyshev-Ritz method to determine the natural frequencies of cantilever rotating composite cylindrical shells made of a polymer matrix reinforced with functionally graded GPLs, based on FSDT. Barati *et al*. (2019) analyzed the free vibration of metal foam shells reinforced with GPLs, applying a first-order shell model Using the multiple scale method (MSM), Wang *et al*. (2019) investigated the nonlinear free vibrations of cylindrical shells reinforced with GPLs and porosity to obtain the nonlinear frequencies. Wu *et al*. (2020) utilized the incremental harmonic balance method (IHBM) to solve the governing differential equation of cylindrical CNT-reinforced shells, adhering to Volmir's assumptions. Yadav *et al*. (2021) established the nonlinear governing differential equations of sandwich cylindrical shells using higher-order shear deformation theory, solved with the aid of IHBM. Abdollahi *et al*. (2022) examined the nonlinear vibrational characteristics of cylindrical shells coupled with a fluid medium using the Runge-Kutta direct integration procedure. Dong *et al*. (2022) considered the nonlinear multi-mode vibrational behaviors of thin-walled cylindrical shells. Marin *et al*. (2014) have tried to extend the domain of influence result to cover the micropolar thermoelastic diffusion. Bhatti *et al*. (2023) study the behavior of hybrid nanofluid flow using a model based on third-grade sodium alginate. The investigation of the reflection issue in a hygrothermal medium in nonlocal elasticity conducted by Yadav *et al*. (2024). Wang *et al*. (2023) employed the Rayleigh-Ritz method and temperature-dependent material properties to ascertain the vibrational characteristics of cylindrical shells with arbitrary boundary conditions in a thermal medium using the Spectral-Geometry method. Recent studies focus on the vibration and buckling characteristics of functionally graded materials (FGM) and composites. Bouafia *et al*. (2021) examined natural frequencies of FGM nanoplates in elastic media, while Khadir *et al*. (2021) analyzed buckling and vibration of FGM carbon nanotube composites. Dai *et al*. (2021) explored frequency characteristics of size-dependent laminated cylindrical nanoshells under thermal loading. Ebrahimi *et al*. (2019) studied curved magneto-electro-viscoelastic nanobeams, and Boutaleb *et al*. (2019) investigated the dynamic response of FGM rectangular nanoplates. Recent work by Mohammed *et al*. (2024) focused on vibrating sandwich cylindrical shells with damaged cores, and Hatami *et al*. (2024) employed a finite strip method for natural frequencies of FGM-carbon nanotube plates. Liu *et al*. (2024) researched composite cylindrical shell vibrations, while Alnujaie *et al*. (2024) analyzed free vibration responses of plates to enhance understanding of material variations in structural engineering. Shen *et al*. (2024) examined free vibration of FG porous spherical caps on elastic foundations. Tahouneh *et al*. (2019) used trimming technique to create the cutout in geometry of L-shape plate. These authors investigated vibration of a single layered graphene sheet (SLGS) based on the nonlocal elasticity model framework of classical Kirchhoff thin plate. Ameer *et al*. (2024) studied free vibration behavior of trapezoidal shaped coupled double-layered graphene sheets (DLGS) system using first-order shear deformation theory (FSDT) and incorporating nonlocal elasticity theory. Tahouneh *et al*. (2020) studied vibration of vacancy defected graphene sheet as a nonisotropic structure via molecular dynamic and continuum approaches. Wu and Liu (2016) developed a state space differential reproducing kernel (DRK) method in order to study 3D analysis of FG circular plates. Marin (2010) considered a right cylinder composed of a physically dipolar thermoelastic material for which one plane end was subjected to an excitation which is harmonic in time. Marin *et al*. (2022) used a linear theory for the thermoelasticity of type III for Cosserat media. Abo-Dahab *et al*. (2020) used the generalized thermoelasticity theory, with one thermal relaxation time (TR), to examine the thermoelastic problem of a functionally graded thin slim strip (TSS). Tornabene (2009) used four-parameter power-law distribution to study the dynamic behavior of moderately thick functionally graded conical and cylindrical shells. Tornabene and Ceruti (2013) studied a mixed static and dynamic optimization of four-parameter functionally graded material (FGM) doubly curved shells and panels. Tornabene *et al*. (2014) studied free vibration of free-form doubly-curved shells made of functionally graded materials using higher-order equivalent single layer theories. The partial differential system of equations was solved by using the Generalized Differential Quadrature (GDQ) method. A multiscale approach is employed to evaluate the overall mechanical properties of the three phase composite face-sheets (Tornabene *et al*. 2019). Chu *et al*. (2023) theoretically evaluated the impacts of moving load and the use of a piezoelectric patch on the level of energy harvesting and dynamic behavior of a Nano Conical Panel (NCP) made from SMA located on a frictional substrate using the First-order Shear Deformation Theory (FSDT). Chu presented (2023) presented energy absorption, and forced and free vibrations of sandwich non-rectangular nanoplates with a single sinusoidal edge resting on a fractional torsional viscoelastic medium. Chu *et al*. (2022) investigated the effect of hole notched in fracture mechanics of GLARE and GFRP composites subjected to quasi-static loading.

Researchers have developed models of microstructures utilizing MCST and SGT, with several investigations aimed at analyzing size-dependent vibrational responses of microplates and microshells. Beni *et al*. (2015) studied the size-dependent vibrations of functionally graded cylindrical shells using a shear deformation model and MCST. Gholami *et al*. (2016) explored the dynamics of micro- and nanoshells employing strain gradient formulations and MCST. Tohidi *et al*. (2017) examined the dynamic stability of FG-CNT-reinforced microshells subjected to harmonic non-uniform temperature distributions. Veysi *et al*. (2017) derived the frequency responses of thick microshells based on Hamilton's principle using MCST and applying the multiple scale method. Hasrati *et al*. (2018) developed a novel numerical solution to characterize the nonlinear free and forced vibrations of cylindrical shells based on FSDT and von Kármán relations. The natural frequencies of cylindrical sandwich micropanels with GPL-reinforced

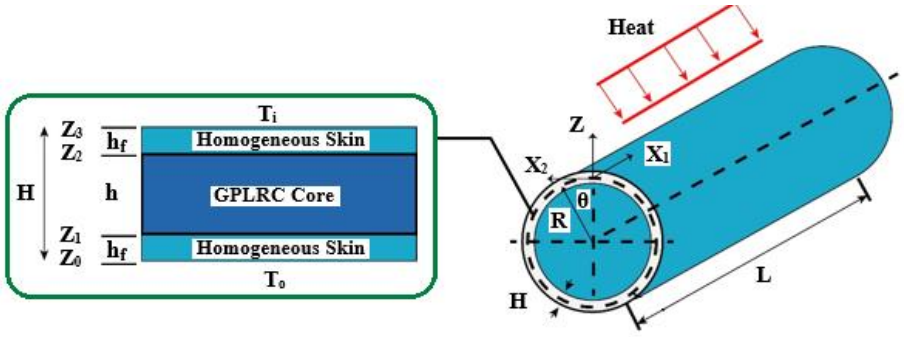

Fig. 1 Schematic of cylindrical shell in thermal medium

layers resting on elastic foundations in thermal environments were studied by Anvari *et al*. (2020) based on MCST using Navier's method. Bidzard *et al*. (2022) employed the harmonic balance method and size-dependent finite element relations to determine the nonlinear frequencies of multilayer FG-GPL-reinforced toroidal microshells resting on a nonlinear elastic foundation in thermal environments, deriving formulations based on modified strain gradient theory, FSDT, and von Kármán assumptions. Utilizing state-space techniques and the fourth-order Runge-Kutta method, Yin and Fang (2023) obtained natural frequencies and dynamic responses for spinning FG-GPL-reinforced microplates based on MCST and FSDT. Ma *et al*. (2024) investigated the bending behavior of GPL-reinforced cylindrical microcapsules subjected to moving loads.

Through a comprehensive literature survey, it becomes evident that there is currently no published study addressing the size-dependent nonlinear vibrations of cylindrical microshells in thermal environments, particularly those made of an FG-GPL-reinforced core, utilizing analytical methods. Nonetheless, the temperature field and size dependence of the microshell structure will undoubtedly influence the vibrational performance of cylindrical sandwich shells with an FG-GPL-reinforced core. Inspired by this gap, the present study investigates the size-dependent nonlinear vibrations of cylindrical sandwich microshells in thermal environments. The shells are modeled by considering shear deformation and rotary inertia along with geometrical nonlinearity, and the governing equations of the sandwich microshell are derived. Subsequently, employing analytical methods, the nonlinear frequencies are analyzed.

2. Mathematical modeling and relations

2.1 Sandwich shell with GPL reinforced core in thermal medium

Fig. 1 represents a sandwich microshell made of a FG-GPL reinforced core with thickness h and two uniform faces with thickness h_f . As shown, L, R, and H denote the length, radius, and shell thickness of the cylindrical shell, respectively. Inner surface (z_0 = -H/2) and outer surface (z_3= H/2) of the shell have been assumed to be pure metal and the two interfaces with FG-GPL reinforced core are at the positions z_1, z_2. Furthermore, The thermal boundary conditions at the inner and outer surface of the shell are: $T(z=z_0) = T_i$ and $T(z=h_3) = T_o$. Because of the GPL dispersion patterns, the varied GPLs volume fraction along the core thickness, as depicted in Fig. 2 are expressed as:

$$\begin{Bmatrix} g_1(z) \\ g_2(z) \\ g_3(z) \end{Bmatrix} = \begin{bmatrix} 1 \\ 1-\cos\left(\frac{\pi z}{h}\right) \\ 1-\cos\left(\frac{\pi z}{2h}+\frac{\pi}{4}\right) \end{bmatrix} \xrightarrow{related\ to} \begin{bmatrix} \text{GPL}-\text{U} \\ \text{GPL}-\text{S} \\ \text{GPL}-\text{A} \end{bmatrix} \tag{1}$$

where $g_i(z)$ $(i = 1,2,3)$ are the shape function of GPL. Also the function of GPL volume fraction is $V_{gpl} = S_i g_i(z)$, in which S_i is the peak values of GPLs volume fraction and can be calculated by (Rafiee *et al*. 2009):

$$S_i \int_{-h/2}^{h/2} g_i(z)dz = \frac{h\, g_{GPL}}{g_{GPL} + (1 - W_{GPL})\rho_{GPL}/\rho_M} \tag{2}$$

In which g_{GPL} is the weight fraction of GPLs. ρ_{GPL} and ρ_M represent the mass densities of GPL and matrix, respectively. Young's modulus of the GPL reinforced core can be calculated by the Halpin-Tsai micromechanics algorithm (Rafiee *et al*. 2009), yielding:

$$E_c = E_M\left[\frac{3}{8}\left(\frac{1+2\xi_L\eta_L V_{GPL}}{1-\eta_L V_{GPL}}\right)+\frac{5}{8}\left(\frac{1+2\xi_B\eta_B V_{GPL}}{1-\eta_B V_{GPL}}\right)\right] \tag{3}$$

In which:

$$\xi_L = \frac{l_{GPL}}{t_{GPL}}, \xi_B = \frac{b_{GPL}}{t_{GPL}},$$
$$\eta_L = \frac{E_{GPL}/E_M - 1}{E_{GPL}/E_M + 2\xi_L}, \tag{4}$$
$$\eta_B = \frac{E_{GPL}/E_M - 1}{E_{GPL}/E_M + 2\xi_B}$$

where l_{GPL}, b_{GPL}, and t_{GPL} are the GPLs' average length, width, and thickness, respectively. E_M and E_{GPL} are elastic moduli of the matrix and GPL materials of core, respectively. In addition, on the basis of the rule of mixture, the Poisson's ratio, thermal expansion and density of the GPLs reinforced matrix of core are defined as:

$$\begin{aligned} \upsilon_c &= \upsilon_{GPL}V_{GPL} + \upsilon_M(1 - V_{GPL}) \\ \alpha_c &= \alpha_{GPL}V_{GPL} + \alpha_M(1 - V_{GPL}) \\ \rho_c &= \rho_{GPL}V_{GPL} + \rho_M(1 - V_{GPL}) \end{aligned} \tag{5}$$

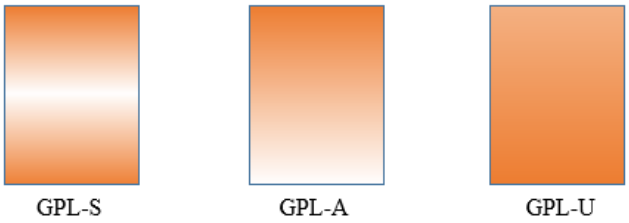

Fig. 2 Distribution of different GPL patterns of the core

In which υ_m , υ_{GPL} are the Poisson's ratios of the matrix and GPLs nanofillers, respectively. Also α_M and α_{GPL} are the thermal expansion of the matrix and GPLs of core, respectively. The thermal conductivity coefficient of the GPLs reinforced composite is:

$$k_c = k_M\left\{1+\frac{V_{GPL}}{3}\left[\left(\frac{2}{H+1/(\frac{k_x}{k_M}-1)}+\frac{1}{(1-H)/2+1/(\frac{k_z}{k_M}-1)}\right)+1\right]\right\},$$
$$H=\frac{Ln\left[\left(\xi_L+\sqrt{{\xi_L}^2-1}\right)\xi_L\right]}{\sqrt{\left({\xi_L}^2-1\right)^3}}-\frac{1}{{\xi_L}^2-1} \quad (6)$$

Besides, in the Eq. (6), k_z and k_x are the thermal conductivity coefficients of the GPLs through the thickness and inplane directions respectively, as:

$$k_x=\frac{k_{GPL}}{1+2R_Kk_{GPL}/l_{GPL}};\ k_z=\frac{k_{GPL}}{1+2R_Kk_{GPL}/t_{GPL}} \quad (7)$$

where k_{GPL} is the thermal conductivity of the GPL along the in-plane direction and R_k is the average interfacial thermal resistance between the GPL and the matrix.

As mentioned, the thermal boundary conditions at the inner and outer surface of microshell are: $T(z=h_0)=T_i$ and $T(z=h_3)=T_o$, So the temperature variation along the shell thickness can be obtained by solving the one-dimentional fourier law of heat conduction $-\frac{d}{dz}\left(K(z)\frac{dT(z)}{dz}\right)=0$. The temperature distribution of sandwich plate is obtained as (Yang *et al*. 2017):

$$T(z)=T_0+(T_o-T_i)\,\Theta_{(n)}\ ;\ \ n=1,2,3 \quad (8)$$

In which T_0 represents the initial temperature under the free stress state, and $\Theta_{(n)}$ denotes the nondimensional temperatures change in the n-th layer; equals to:

$$\Theta_{(1)}=\frac{\int_{h_0}^{z}\frac{dz}{K_{(1)}}}{\sum_{n=1}^{3}\int_{h_{n-1}}^{h_n}\frac{dz}{K_{(n)}}}\ ;\ \ z\in[z_0,z_1]$$
$$\Theta_{(2)}=\frac{\int_{h_0}^{h_1}\frac{dz}{K_{(1)}}+\int_{h_1}^{z}\frac{dz}{K_{(2)}}}{\sum_{n=1}^{3}\int_{h_{n-1}}^{h_n}\frac{dz}{K_{(n)}}}\ ;\ \ z\in[z_1,z_2] \quad (9)$$
$$\Theta_{(3)}=\frac{\int_{h_0}^{h_1}\frac{dz}{K_{(1)}}+\int_{h_1}^{h_2}\frac{dz}{K_{(2)}}+\int_{h_2}^{z}\frac{dz}{K_{(3)}}}{\sum_{n=1}^{3}\int_{h_{n-1}}^{h_n}\frac{dz}{K_{(n)}}}\ ;\ \ z\in[z_2,z_3]$$

where $K_{(i)}$, i=1,2,3 is the thermal conductivity coefficient of the i-th layer. The solution of the previous formulation can be obtained by means of polynomial series.

2.2 Governing Equation of sandwich microshell using MCST

An orthogonal coordinate system (x_1, x_2, z) is adopted. u_0, v_0, and w_0 are components of displacements of the middle surface ($z=0$) in the x, θ, and z-directions, respectively. Consistent with the shear deformation assumptions, the displacement field generally expressed as follows:

$$\begin{gathered}u_1(x_1,x_2,z,t)=u(x_1,x_2,t)+z\phi_1(x_1,x_2,t)\\ v_1(x_1,x_2,z,t)=v(x_1,x_2,t)+z\phi_2(x_1,x_2,t)\\ w_1(x_1,x_2,z,t)=w(x_1,x_2,t)\end{gathered} \quad (10)$$

where (u, v, w) are the midsurface displacements at coordinate (x_1, x_2, 0) of cylindrical micro shell, (ϕ_1, ϕ_2) normal rotations. Using the above displacement field and nonlinear shell theory, the mid-surface strains (membrane and shear strain) and curvature can be obtained. The geometrically nonlinear membrane strain, and the transverse shear strains and curvatures are given by adding the von Kármán terms to the linear strain– displacement relations:

$$\begin{gathered}\varepsilon_1=\frac{\partial u}{\partial x_1}+\frac{1}{2}\left(\frac{\partial w}{\partial x_1}\right)^2\\ \varepsilon_2=\frac{1}{R}\left(\frac{\partial v}{\partial x_2}+w\right)+\frac{1}{2}\left(\frac{1}{R}\frac{\partial w}{\partial x_2}\right)^2\\ \varepsilon_{12}=\frac{\partial v}{\partial x_1}+\frac{1}{R}\frac{\partial u}{\partial x_2}+\frac{1}{R}\frac{\partial w}{\partial x_1}\frac{\partial w}{\partial x_2}\\ \varepsilon_{13}=\frac{\partial w}{\partial x_1}+\phi_1\ ,\varepsilon_{23}=\frac{1}{R}\frac{\partial w}{\partial x_2}+\phi_2\\ \kappa_1=\frac{\partial\phi_1}{\partial x_1}\ ,\kappa_2=\frac{1}{R}\frac{\partial\phi_2}{\partial x_2}\\ \kappa_{12}=\frac{\partial\phi_2}{\partial x_1}+\frac{1}{R}\frac{\partial\phi_1}{\partial x_2}\end{gathered} \quad (11)$$

According to MCST and considering scale effect, the virtual strain energy can be obtained by integrating over the entire volume of cylindrical micro shell:

$$U_s=\frac{1}{2}\int_s\left[\begin{array}{l}\int_{-\frac{h}{2}}^{\frac{h}{2}}\left(\sigma_{ij}^c\delta\varepsilon_{ij}+m_{ij}^c\delta\chi_{ij}\right)R\,dx_1dx_2\\ +\int_{-\frac{h}{2}}^{-\frac{h}{2}}\left(\sigma_{ij}^f\delta\varepsilon_{ij}+m_{ij}^f\delta\chi_{ij}\right)R\,dx_1dx_2\\ +\int_{h/2}^{h/2}\left(\sigma_{ij}^f\delta\varepsilon_{ij}+m_{ij}^f\delta\chi_{ij}\right)R\,dx_1dx_2\end{array}\right]dz \quad (12)$$

where σ_{ij}^c and σ_{ij}^f are, respectively, the stress components of the κ-layer (κ = c, f) are related to the corresponding strain components as:

$$\sigma^c=[\sigma_{11}^c\ \sigma_{22}^c\ \sigma_{12}^c\ \sigma_{23}^c\ \sigma_{13}^c]^T=\Upsilon^c(z)[\varepsilon-\alpha^c(z)\Delta T^c]$$
$$\sigma^f=\left[\sigma_{11}^f\ \sigma_{22}^f\ \sigma_{12}^f\ \sigma_{23}^f\ \sigma_{13}^f\right]^T=\Gamma^f[\varepsilon-\alpha^f\Delta T^f] \quad (13)$$

In which $\boldsymbol{\varepsilon}=[\varepsilon_{11}\ \varepsilon_{22}\ \varepsilon_{12}\ \varepsilon_{23}\ \varepsilon_{13}]^T$ are the strain components. Besides $\boldsymbol{\alpha}^c(z)=[\alpha_1^c(z)\ \alpha_2^c(z)\ 0\ 0\ 0]^T$ and $\alpha^f=\left[\alpha_1^f\ \alpha_2^f\ 0\ 0\ 0\right]^T$. Also $\Upsilon^c(z)$ and Γ^f are the matrices of

stiffness coefficients for composite core and face layers, respectively, defined according to:

$$\begin{gathered}\Upsilon_{11}^{c}=\Upsilon_{22}^{c}=\frac{E^{c}(z)}{1-\upsilon^{c}(z)^{2}}\,,\\ \Upsilon_{12}^{c}=\frac{\upsilon^{c}(z)E^{c}(z)}{1-\upsilon^{c}(z)^{2}}\,,\\ \Upsilon_{44}^{c}=\Upsilon_{55}^{c}=\Upsilon_{66}^{c}=\frac{E^{c}(z)}{2\left(1+\upsilon^{c}(z)\right)}\\ \Upsilon_{11}^{f}=\Upsilon_{22}^{f}=\frac{E^{f}}{1-\upsilon^{f\,2}}\,,\\ \Upsilon_{22}^{f}=\frac{\upsilon^{f}E^{f}}{1-\upsilon^{f\,2}}\,,\\ \Upsilon_{44}^{f}=\Upsilon_{55}^{f}=\Upsilon_{66}^{f}=\frac{E^{f}}{2(1+\upsilon^{f})}\end{gathered}\tag{14}$$

The strains $\boldsymbol{\varepsilon}$ at arbitrary point (x, θ, z) can be obtained by mid-surface strains and curvatures.

Beside the thermal expansion coefficients ($\alpha_{11}^{f}\ \alpha_{22}^{f}$) of longitudinal and circumferential directions (x, θ) for the face layers are assumed to be equal $\alpha_{11}^{f}=\alpha_{22}^{f}=\alpha^{f}$.

Moreover, m_{ij}^{c} and m_{ij}^{f} denote the higher-order stress components of the κ-layer (κ = c, f) for core layer and surface layers, respectively. Also χ_{ij} represent the curvature tensor of strain energy, in which:

$$\begin{aligned}m_{ij}^{c}&=2l^{2}\Upsilon_{66}^{c}\chi_{ij};\ \ (i,j=1,2,3)\\ m_{ij}^{f}&=2l^{2}\Upsilon_{66}^{f}\chi_{ij};\ \ (i,j=1,2,3)\end{aligned}\tag{15}$$

where l is the material length scale (LS) parameter of both core and face layers. Using the geometric characteristics of the thin shell ($1+z/R=1$), and the displacement field of shear deformation shell, the curvature tensor χ_{ij} (nonzero) in this case are:

$$\begin{aligned}\chi_{11}&=\frac{1}{2R}\left(\frac{\partial^{2}w}{\partial x_{1}\partial x_{2}}-\frac{\partial v}{\partial x_{1}}\right)-\frac{1}{2}\frac{\partial\phi_{2}}{\partial x_{1}}\\ \chi_{22}&=\frac{1}{2R}\left(\frac{\partial\phi_{1}}{\partial x_{2}}-\frac{\partial^{2}w}{\partial x_{1}\partial x_{2}}+\frac{\partial v}{\partial x_{1}}+z\frac{\partial\phi_{2}}{\partial x_{1}}-\frac{1}{R}\frac{\partial u}{\partial x_{2}}\right)\\ \chi_{33}&=\frac{1}{2}\left[\frac{\partial\phi_{2}}{\partial x_{1}}-\frac{1}{R}\left(\frac{\partial\phi_{1}}{\partial x_{2}}-\frac{1}{R}\frac{\partial u}{\partial x_{2}}\right)\right]\\ \chi_{12}=\chi_{21}&=\frac{1}{4}\begin{bmatrix}\dfrac{\partial\phi_{1}}{\partial x_{1}}-\dfrac{\partial^{2}w}{\partial x_{1}^{2}}-\dfrac{1}{R}\dfrac{\partial\phi_{2}}{\partial x_{2}}\\ +\dfrac{1}{R^{2}}\left(\dfrac{\partial^{2}w}{\partial x_{2}^{2}}-\dfrac{\partial v}{\partial x_{2}}\right)\end{bmatrix}\\ \chi_{13}&=\chi_{31}\\ &=\frac{1}{4}\begin{bmatrix}\dfrac{\partial^{2}v}{\partial x_{1}^{2}}+z\dfrac{\partial^{2}\phi_{2}}{\partial x_{1}^{2}}+\dfrac{1}{R}\left(-\dfrac{\partial^{2}u}{\partial x_{1}\partial x_{2}}-z\dfrac{\partial^{2}\phi_{1}}{\partial x_{1}\partial x_{2}}\right)\\ -\dfrac{1}{R}\phi_{2}+\dfrac{1}{R^{2}}\left(v-\dfrac{\partial w}{\partial x_{2}}\right)\end{bmatrix},\\ \chi_{23}=\chi_{32}&=\frac{1}{4}\begin{bmatrix}\frac{1}{R}\left(\frac{\partial^{2}v}{\partial x_{1}\partial x_{2}}+z\frac{\partial^{2}\phi_{2}}{\partial x_{1}\partial x_{2}}-\phi_{1}+\frac{\partial w}{\partial x_{1}}\right)\\ -\frac{1}{R^{2}}\left(\frac{\partial^{2}u}{\partial x_{2}^{2}}+z\frac{\partial^{2}\phi_{1}}{\partial x_{2}^{2}}\right)\end{bmatrix},\end{aligned}\tag{16}$$

For the microshell, the virtual kinetic energy of the sandwich microshell can be given by:

$$\begin{aligned}&\delta K\\ &=\int_{S}\left[\int_{-\frac{h}{2}}^{\frac{h}{2}}\rho^{c}(z)\begin{bmatrix}(\dot{u}+z\dot{\phi}_{1})(\delta\dot{u}+z\delta\dot{\phi}_{1})\\ +(\dot{v}+z\dot{\phi}_{2})(\delta\dot{v}+z\delta\dot{\phi}_{2})+\dot{w}\delta\dot{w}\end{bmatrix}Rdz\right.\\ &+\int_{-\frac{H}{2}}^{\frac{-h}{2}}\rho^{f}\begin{bmatrix}(\dot{u}+z\dot{\phi}_{1})(\delta\dot{u}+z\delta\dot{\phi}_{1})\\ +(\dot{v}+z\dot{\phi}_{2})(\delta\dot{v}+z\delta\dot{\phi}_{2})+\dot{w}\delta\dot{w}\end{bmatrix}Rdz\\ &\left.+\int_{\frac{h}{2}}^{\frac{H}{2}}\rho^{f}\begin{bmatrix}(\dot{u}+z\dot{\phi}_{1})(\delta\dot{u}+z\delta\dot{\phi}_{1})\\ +(\dot{v}+z\dot{\phi}_{2})(\delta\dot{v}+z\delta\dot{\phi}_{2})+\dot{w}\delta\dot{w}\end{bmatrix}Rdz\right]dx_{1}dx_{2}\end{aligned}\tag{17}$$

Next, Hamilton's principle (the dynamic version of the principle of virtual displacements) is employed.

$$\delta\int_{t_{1}}^{t_{2}}(K-U_{s})dt=0\tag{18}$$

By substituting Eqs. (12-17) into Eq. (18) and letting the coefficients in front of δu, δv, δw, $\delta\phi_{1}$, and $\delta\phi_{2}$ to be zero, respectively, the nonlinear dynamic governing equations in the partial differential form can be obtained as:

$$\begin{aligned}\delta u:\ &\frac{\partial N_{1}}{\partial x_{1}}+\frac{1}{R}\frac{\partial N_{12}}{\partial x_{2}}-\frac{1}{2R^{2}}\frac{\partial Y_{22}}{\partial x_{2}}+\frac{1}{2R^{2}}\frac{\partial Y_{33}}{\partial x_{2}}\\ &+\frac{1}{2R}\frac{\partial^{2}Y_{13}}{\partial x_{1}\partial x_{2}}+\frac{1}{2R^{2}}\frac{\partial^{2}Y_{23}}{\partial x_{2}^{2}}=I_{0}\ddot{u}+I_{1}\ddot{\phi}_{1}\end{aligned}\tag{19a}$$

$$\begin{aligned}\delta v:\ &\frac{1}{R}\frac{\partial N_{2}}{\partial x_{2}}+\frac{\partial N_{12}}{\partial x_{1}}+\frac{1}{R}Q_{2}-\frac{1}{2R}\frac{\partial Y_{11}}{\partial x_{1}}+\frac{1}{2R}\frac{\partial Y_{22}}{\partial x_{1}}\\ &-\frac{1}{2R^{2}}\frac{\partial Y_{12}}{\partial x_{2}}-\frac{1}{2}\frac{\partial^{2}Y_{13}}{\partial x_{1}^{2}}-\frac{1}{2R^{2}}Y_{13}-\frac{1}{2R}\frac{\partial^{2}Y_{23}}{\partial x_{1}\partial x_{2}}\\ &=I_{0}\ddot{v}+I_{1}\ddot{\phi}_{2}\end{aligned}\tag{19b}$$

$$\begin{aligned}\delta w:\ &\frac{\partial Q_{2}}{\partial x_{2}}+\frac{\partial Q_{1}}{\partial x_{1}}-\frac{1}{R}N_{2}+\eta(u,v,w,\phi_{1},\phi_{2})\\ &-\frac{1}{2R}\frac{\partial^{2}Y_{11}}{\partial x_{1}\partial x_{2}}+\frac{1}{2R}\frac{\partial^{2}Y_{22}}{\partial x_{1}\partial x_{2}}-\frac{1}{2R^{2}}\frac{\partial^{2}Y_{12}}{\partial x_{2}^{2}}\\ &+\frac{1}{2}\frac{\partial^{2}Y_{12}}{\partial x_{1}^{2}}-\frac{1}{2R^{2}}\frac{\partial Y_{13}}{\partial x_{2}}+\frac{1}{2R}\frac{\partial Y_{23}}{\partial x_{1}}=I_{0}\ddot{w}\end{aligned}\tag{19c}$$

$$\begin{aligned}\phi_{1}:\ &\frac{\partial M_{1}}{\partial x_{1}}+\frac{1}{R}\frac{\partial M_{12}}{\partial x_{2}}-Q_{1}+\frac{1}{2R}\frac{\partial Y_{22}}{\partial x_{2}}+\frac{1}{2R}\frac{\partial Y_{33}}{\partial x_{2}}\\ &+\frac{1}{2}\frac{\partial Y_{12}}{\partial x_{1}}+\frac{1}{2R}\frac{\partial^{2}T_{13}}{\partial x_{2}^{2}}+\frac{1}{2R}Y_{23}=I_{1}\ddot{u}+I_{2}\ddot{\phi}_{1}\end{aligned}\tag{19d}$$

$$\begin{aligned}\phi_{2}:\ &\frac{1}{R}\frac{\partial M_{2}}{\partial x_{2}}+\frac{\partial M_{12}}{\partial x_{1}}-Q_{2}-\frac{1}{2}\frac{\partial Y_{11}}{\partial x_{1}}+\frac{1}{2R}\frac{\partial T_{22}}{\partial x_{1}}\\ &+\frac{1}{2}\frac{\partial Y_{12}}{\partial x_{2}}-\frac{1}{2}\frac{\partial^{2}T_{13}}{\partial x_{1}^{2}}+\frac{1}{2R}Y_{13}-\frac{1}{2R}\frac{\partial^{2}T_{23}}{\partial x_{1}\partial x_{2}}\\ &=I_{1}\ddot{v}+I_{2}\ddot{\phi}_{2}\end{aligned}\tag{19e}$$

In which, the mass moments are equal to:

$$I_{j}=\int_{-h/2}^{h/2}\rho^{c}(z)\left(1+\frac{z}{R}\right)z^{i}dz+\int_{-H/2}^{-h/2}\rho^{f}\left(1+\frac{z}{R}\right)z^{i}dz+\int_{h/2}^{H/2}\rho^{f}(1+z/R)z^{i}dz\,;\quad(j=0,1,2)$$

The nonlinear expression $\eta(u,v,w,\phi_{1},\phi_{2})$ is the nonlinear contribution to the equilibrium equations due to the von karman nonlinear strains can give by:

$$\eta(u,v,w,\phi_1,\phi_2)=\frac{\partial}{\partial x_1}\left(N_1\frac{\partial w}{\partial x_1}\right)+\frac{1}{R^2}\frac{\partial}{\partial x_2}\left(N_2\frac{\partial w}{\partial x_2}\right)+\frac{1}{R}\frac{\partial}{\partial x_2}\left(N_{12}\frac{\partial w}{\partial x_1}\right)+\frac{1}{R}\frac{\partial}{\partial x_1}\left(N_{12}\frac{\partial w}{\partial x_2}\right) \quad (20)$$

The stress resultants $(N_1, N_2,\ N_{12})$, $(M_1, M_2,\ M_{12})$ and (Q_1, Q_2) with thermal effects and the couple stress higher-order stress resultants $Y_{ij},\ T_{ij}$ can also be given as:

$$\begin{Bmatrix}N_1\\N_2\\N_{12}\end{Bmatrix}=\begin{bmatrix}A_{11}&A_{12}&0\\A_{21}&A_{22}&0\\0&0&A_{66}\end{bmatrix}\begin{Bmatrix}\varepsilon_1\\\varepsilon_2\\\varepsilon_{12}\end{Bmatrix}+\begin{bmatrix}B_{11}&B_{12}&0\\B_{21}&B_{22}&0\\0&0&B_{66}\end{bmatrix}\begin{Bmatrix}\kappa_1\\\kappa_2\\\kappa_{12}\end{Bmatrix}-\begin{Bmatrix}N_1^T\\N_2^T\\N_{12}^T\end{Bmatrix}$$

$$\begin{Bmatrix}M_1\\M_2\\M_{12}\end{Bmatrix}=\begin{bmatrix}B_{11}&B_{12}&0\\B_{21}&B_{22}&0\\0&0&B_{66}\end{bmatrix}\begin{Bmatrix}\varepsilon_1\\\varepsilon_2\\\varepsilon_{12}\end{Bmatrix}+\begin{bmatrix}D_{11}&D_{12}&0\\D_{21}&D_{22}&0\\0&0&D_{66}\end{bmatrix}\begin{Bmatrix}\kappa_1\\\kappa_2\\\kappa_{12}\end{Bmatrix}-\begin{Bmatrix}M_1^T\\M_2^T\\M_{12}^T\end{Bmatrix} \quad (21)$$

$$\begin{Bmatrix}Q_1\\Q_2\end{Bmatrix}=\begin{bmatrix}E_{44}&0\\0&E_{55}\end{bmatrix}\begin{Bmatrix}\varepsilon_{13}\\\varepsilon_{23}\end{Bmatrix}$$

In which the thermal resultants are:

$$\left\langle\begin{Bmatrix}N_1^T\\N_2^T\\N_{12}^T\end{Bmatrix},\begin{Bmatrix}M_1^T\\M_2^T\\M_{12}^T\end{Bmatrix}\right\rangle = \int_{-h/2}^{h/2}\begin{Bmatrix}Q_{11}^c(z)\alpha_1^c(z)+Q_{22}^c(z)\alpha_2^c(z)\\Q_{12}^c(z)\alpha_1^c(z)+Q_{22}^c(z)\alpha_2^c(z)\\0\end{Bmatrix}\Delta T^c\langle 1,z\rangle dz + \int_{-H/2}^{-h/2}\begin{Bmatrix}Q_{11}^f\alpha_1^f+Q_{22}^f\alpha_2^f\\Q_{12}^f\alpha_1^f+Q_{22}^f\alpha_2^f\\0\end{Bmatrix}\Delta T^f\langle 1,z\rangle dz + \int_{h/2}^{H/2}\begin{Bmatrix}Q_{11}^f\alpha_1^f+Q_{22}^f\alpha_2^f\\Q_{12}^f\alpha_1^f+Q_{22}^f\alpha_2^f\\0\end{Bmatrix}\Delta T^f\langle 1,z\rangle dz \quad (22)$$

where:

$$\langle Y_{ij},T_{ij}\rangle=\int_{-\frac{h}{2}}^{\frac{h}{2}}m_{ij}^c\langle 1,z\rangle dz+\int_{-\frac{H}{2}}^{-\frac{h}{2}}m_{ij}^f\langle 1,z\rangle dz+\int_{h/2}^{H/2}m_{ij}^f\langle 1,z\rangle dz$$

$$\{A_{ij},B_{ij},D_{ij}\}=\int_{-\frac{h}{2}}^{\frac{h}{2}}Q_{ij}^c(z)\{1,z,z^2\}dz+\int_{-\frac{H}{2}}^{-\frac{h}{2}}Q_{ij}^f\{1,z,z^2\}dz+\int_{\frac{h}{2}}^{\frac{H}{2}}Q_{ij}^f\{1,z,z^2\}dz \quad (23)$$

$$\{E_{44},E_{55}\}=\int_{-\frac{h}{2}}^{\frac{h}{2}}\{Q_{44}^c(z),Q_{55}^c(z)\}dz+\int_{-H/2}^{-h/2}\{Q_{44}^f,Q_{55}^f\}dz+\int_{h/2}^{H/2}\{Q_{44}^f,Q_{55}^f\}dz$$

In which the effective elasticity coefficients $Q_{ij}^c,\ Q_{ij}^f$ related to the cylindrical shell are given as:

$$Q_{11}^{c,f}=\Upsilon_{11}^{c,f};\ Q_{12}^{c,f}=\frac{\Upsilon_{12}^{c,f}}{(1+z/R)};\quad Q_{22}^{c,f}=\frac{\Upsilon_{22}^{c,f}}{(1+z/R)};\ Q_{44}^{c,f}=\kappa_1\Upsilon_{44}^{c,f};\quad Q_{55}^{c,f}=\kappa_2\frac{\Upsilon_{55}^{c,f}}{(1+z/R)};\ Q_{66}^{c,f}=\frac{\Upsilon_{66}^{c,f}}{(1+z/R)} \quad (24)$$

In which $\kappa_1,\ \kappa_2$ are modified shear correction factors and equals to $\kappa_1=\kappa_2=5/6$.

The five coupled Eqs. (19a-19e) can be transformed with the midsurface displacements (u, v, w) and rotations $(\phi_1,\ \phi_2)$. Then, for sandwich cylindrical microshell, the equations of motion take the form:

$$L_{11}u+L_{12}v+L_{13}w+L_{14}\phi_1+L_{15}\phi_2+l^2\left(L_{11}^l u+L_{12}^l v+L_{13}^l w+L_{14}^l\phi_1+L_{15}^l\phi_2\right)+L_{16}ww_1'+L_{17}ww_2'=I_0\ddot{u}+I_1\ddot{\phi}_1 \quad (25a)$$

$$L_{21}u+L_{22}v+L_{23}w+L_{24}\phi_1+L_{25}\phi_2+l^2\left(L_{21}^l u+L_{22}^l v+L_{23}^l w+L_{24}^l\phi_1+L_{25}^l\phi_2\right)+L_{26}ww_1'+L_{27}ww_2'=I_0\ddot{v}+I_1\ddot{\phi}_2 \quad (25b)$$

$$L_{31}u+L_{32}v+L_{33}w+L_{34}\phi_1+L_{35}\phi_2+l^2\left(L_{31}^l u+L_{32}^l v+L_{33}^l w+L_{34}^l\phi_1+L_{35}^l\phi_2\right)+L_{36}ww_1'+L_{37}ww_2'+\eta(u,v,w,\phi_1,\phi_2)+q_z=I_0\ddot{w} \quad (25c)$$

$$L_{41}u+L_{42}v+L_{43}w+L_{44}\phi_1+L_{45}\phi_2+l^2\left(L_{41}^l u+L_{42}^l v+L_{43}^l w+L_{44}^l\phi_1+L_{45}^l\phi_2\right)+L_{46}ww_1'+L_{47}ww_2'=I_1\ddot{u}+I_2\ddot{\phi}_1 \quad (25d)$$

$$L_{51}u+L_{52}v+L_{53}w+L_{54}\phi_1+L_{55}\phi_2+l^2\left(L_{51}^l u+L_{52}^l v+L_{53}^l w+L_{54}^l\phi_1+L_{55}^l\phi_2\right)+L_{56}ww_1'+L_{57}ww_2'=I_1\ddot{v}+I_2\ddot{\phi}_2 \quad (25e)$$

In these equations, L_{ij} and L_{ij}^l algebraic terms are related to material and geometry of the shell.

2.3 Solution procedure

In this section, an analytical method based on Galerkin method and multiple scale perturbation technique is applied to solve the coupled nonlinear vibration equations corresponding to the simply supported cylindrical microshell. In this regard, the mathematical expression of simply supported BCs can present as v = w = M_{11} = $\phi_2 = 0$ at x=0, L. Taking into account simply supported boundary conditions, the displacement variables can be selected as the following form:

$$\begin{aligned}u(x_1,x_2,t)&=U(t)\cos(\lambda_m x)\cos(n\theta)\\v(x_1,x_2,t)&=V(t)\sin(\lambda_m x)\sin(n\theta)\\w(x_1,x_2,t)&=W(t)\sin(\lambda_m x)\cos(n\theta)\\\phi_1(x_1,x_2,t)&=\Phi(t)\,cos(\lambda_m x)\,cos(n\theta)\\\phi_2(x_1,x_2,t)&=\Psi(t)(t)\,sin(\lambda_m x)sin(n\theta)\end{aligned} \quad (26)$$

where the time-dependent variables $U_{mn}(t)$, $V_{mn}(t)$, $W_{mn}(t)$, $\Phi_{mn}(t)$, $\Psi_{mn}(t)$ are coefficients to be determined in the following equation. Also $\lambda_m = m\pi/L$, m and (n=1,2, 3, …) are the half wave numbers corresponding directions x_1 and x_2, respectively. For the sake of brevity, the *mn* indexes have not be written in the next relations.

Using Galerkin's technique and substituting the Eqs. (26) into Eqs. (25a-25e) yields, a set of time-dependent ordinary differential equations (ODEs) can be obtained. Besides, when the transverse flexural motion in such thin-walled structures is assumed to be dominant, a common method is to neglect the inertial terms $\ddot{u}, \ddot{\phi}_1, \ddot{v}, \ddot{\phi}_2$; which has been stated in literature (Ding and She 2023):

$$C_{11}U(t) + C_{12}V(t) + C_{13}W(t) + C_{14}\Phi(t) + C_{15}\Psi(t) + C_{16}W(t)^2 = 0 \quad (27)$$

$$C_{21}U(t) + C_{22}V(t) + C_{23}W(t) + C_{24}\Phi(t) + C_{25}\Psi(t) + C_{26}W(t)^2 = 0 \quad (28)$$

$$C_{31}U(t) + C_{32}V(t) + C_{33}W(t) + C_{34}\Phi(t) + C_{35}\Psi(t) + C_{36}W(t)^2 + C_3^1U(t)W(t) + C_3^2V(t)W(t) + C_3^4\Phi(t)W(t) + C_3^5\Psi(t)W(t) + M_{33}\ddot{W}(t) = 0 \quad (29)$$

$$C_{41}U(t) + C_{42}V(t) + C_{43}W(t) + C_{44}\Phi(t) + C_{45}\Psi(t) + C_{46}W(t)^2 = 0 \quad (30)$$

$$C_{51}U(t) + C_{52}V(t) + C_{53}W(t) + C_{54}\Phi(t) + C_{55}\Psi(t) + C_{56}W(t)^2 = 0 \quad (31)$$

In which, the coefficients C_{ij} have been defined in Appendix A. Now, the static condensation procedure based on Volmir's assumption (Bich and Nguyen 2012) with an acceptable precision is employed to the Eqs. (27, 28) and Eqs.(30, 31), resulting in the next expression:

$$\begin{bmatrix} C_{11} & C_{12} & C_{14} & C_{15} \\ C_{21} & C_{22} & C_{24} & C_{25} \\ C_{41} & C_{42} & C_{44} & C_{45} \\ C_{51} & C_{52} & C_{54} & C_{55} \end{bmatrix} \begin{bmatrix} U \\ V \\ \Phi \\ \Psi \end{bmatrix} = -\begin{bmatrix} C_{13} \\ C_{23} \\ C_{43} \\ C_{53} \end{bmatrix} W - \begin{bmatrix} C_{16} \\ C_{26} \\ C_{46} \\ C_{56} \end{bmatrix} W^2 \quad (32)$$

By solving Eq. (33), the expressions of U, V, Φ and Ψ can be characterized by W, which are:

$$U = K_{uw}W + K_{uww}W^2 V = K_{vw}W + K_{vww}W^2$$
$$\Phi = K_{xw}W + K_{xww}W^2\Psi = K_{yw}W + K_{yww}W^2 \quad (33)$$

In which the coefficients of $K_{\alpha w}$, $K_{\alpha ww}$ (α = u, v, x, y) have been supplemented in Appendix B. Replacing Eq. (33) into Eq. (29), the nonlinear dynamic equations of cylindrical microshell under thermo-mechanical environments subjected to harmonic excitation obtained as:

$$\ddot{W}(t) + K_1W(t) + K_2W(t)^2 + K_3W(t)^3 = 0 \quad (34)$$

where

$$K_1 = -\frac{1}{M_{33}}\left(C_{31}K_{uw} + C_{32}K_{vw} + C_{34}K_{xw} + C_{35}K_{yw} + C_{33}\right)$$
$$K_2 = -\frac{1}{M_{33}}\left(C_{31}K_{uww} + C_3^1K_{uw} + C_{32}K_{vww} + C_3^2K_{vw} + C_{34}K_{xww} + C_3^4K_{xw} + C_{35}K_{yww} + C_3^5K_{yw} + C_{36}\right) \quad (35)$$
$$K_3 = -\frac{1}{M_{33}}\left(C_3^1K_{uww} + C_3^2K_{vww} + C_3^4K_{xww} + C_3^5K_{yyw} + C_{no}\right);$$

Employing Improved Lindstedt-Poincar´e method, an analytical solution has been obtained for the Eq. (34). The initial condition is presumed to be as: $(0) = A_{max} = \frac{W_{max}}{H}$; $\frac{dW}{dt}(0) = 0$. In which, A_{max} represents the non-dimensional maximum vibration amplitude. Besides $\omega = \sqrt{K_1}$ equal to linear natural frequency of the sandwich microshell.

A positive, dimensionless, and small parameter (ϵ) should be defined, to enable the proposed method. The coefficient K_1 and W(t) can then be expressed as a power series of ϵ , as follows:

$$W = W_0 + \epsilon W_1 + \epsilon^2 W_2 + \cdots$$
$$K_1 = \omega^2 + \epsilon k_1 + \epsilon^2 k_2 + \cdots \quad (36)$$

By substituting the relations (36) into Eq. (34) and separating the coefficients:

$$\epsilon^0 : \ddot{W} + \omega^2 W_0 = 0\,;$$
$$W_0(0) = A_{max}\,, \frac{dW_0}{dt}(0) = 0 \quad (37)$$

$$\epsilon^1 : \ddot{W}_1 + \omega^2 W_1 = -k_1W_0 - K_2{W_0}^2 - K_3{W_0}^3\,; \quad W_1(0) = 0, \quad \frac{dW_1}{dt}(0) = 0 \quad (38)$$

$$\epsilon^2 : \ddot{W}_2 + \omega^2 W_2 = -k_2W_0 - k_1W_1 - 2K_2W_0W_1 - 3K_3{W_0}^2W_1; \quad W_2(0) = 0, \quad \frac{dW_2}{dt}(0) = 0 \quad (39)$$

The solution of Eq. (37) is $W_0 = A_{max}\cos(\omega t)$. By substituting this solution into Eq. (38), one can write:

$$\ddot{W}_1 + \omega^2 W_1 = -\left(k_1A_{max} - \tfrac{3}{4}K_3{A_{max}}^3\right)\cos(\omega t) - \tfrac{1}{2}K_2{A_{max}}^2\cos(2\omega t) - \tfrac{1}{2}K_2{A_{max}}^2 \quad (40)$$

By removing the secular terms in Eq. (40), the coefficient k_1 equals to : $k_1 = -\frac{3}{4}K_3{A_{max}}^2$. Therefore the solution of Eq. (40) is as follows:

$$W_1 = -\left(\frac{K_2}{3\omega^2}{A_{max}}^2 - \frac{K_3}{32\omega^2}{A_{max}}^3\right)\cos(\omega t) + \frac{K_2}{6\omega^2}{A_{max}}^2\cos(2\omega t) + \frac{K_3}{32\omega^2}{A_{max}}^3\cos(3\omega t) - \frac{K_2}{2\omega^2}{A_{max}}^2 \quad (41)$$

To obtain the unknown coefficient k_2, the secular terms produced by substituting W_0 and W_1 into equation (40) should be removed, then : $k_2 = \left(\frac{3{K_3}^2}{128\omega^2}\right){A_{max}}^4 - \left(\frac{K_3K_2}{2\omega^2}\right){A_{max}}^3 + \left(\frac{5{K_2}^2}{6\omega^2}\right){A_{max}}^2$. The nonlinear natural frequency of the sandwich microshell can be obtained from Eq. (36) as follows:

$$\omega_{NL} = \sqrt{\left(K_1 + \tfrac{3}{4}\epsilon K_3{A_{max}}^2\right)^2 + \epsilon^2\left(2K_3K_2{A_{max}}^3 - \tfrac{10}{3}{K_2}^2{A_{max}}^2 - \tfrac{3}{32}{K_3}^2{A_{max}}^4\right)} \quad (42)$$

Table 1 Comparison of the linear frequencies for an isotropic shell at different H/R ratio and wave number (n)

H/R	Beni *et al*. (2015)	Gholami *et al*. (2016)	Present
	1.126	1.132	1.135
0.1	1.069	1.074	1.080
	1.207	1.214	1.219
	1.537	1.538	1.571
0.2	1.590	1.601	1.645
	1.928	1.949	2.002

Table 2 Validation of ω_{NL}/ω_L ratio for cylindrical shell at different wave numbers (n)

Model	Mode		
	n=2	n=3	n=4
Present	1.0014	1.0131	1.0765
Wang *et al*. (2019)	1.0009	1.0033	1.0117
Hasrati *et al*. (2018)	1.0010	1.0072	1.0452

Table 3 Mechanical properties of GPLs and the polymer epoxy (Yang *et al*. 2017)

Material	E (GPa)	v	ρ (kg/m^3)	α (×10^{-5})/K	k (W/mK)	R_k (m^{2}K/W)
GPL	1010	0.186	1062	2.35	2000	1×10 $^{-8}$
Epoxy	2.85	0.34	1200	8.4	0.2	

3. Results and discussions

3.1 Validation

For the first case. dimenionless linear natural frequencies ($\bar{\omega}$) of cylindrical microshell made by homogenous material with LS parameter $(l = h)$ have been calculated by MCST, and compared with numerical results from literature for isotropic shells (E=1.06 TPa, ρ=2.3 g⁄cm^3, L/R=1), at Table 1. There is a good agreement between the present results and numerical results obtained by Gholami *et al*. (2016) and Beni *et al*. (2015). ($\bar{\omega} = \omega R\sqrt{\rho/E}$).

For the second case, as shown in Table 2, the nonlinear-to-linear frequency ratios ($\frac{\omega_{NL}}{\omega_L}$) for homogeneous cylindrical microshells with thickness H=2.55mm and Length L = 425 mm have been compared with results of Wang *et al*. (2019) and Hasrati *et al*. (2018), Present results are in good agreement with the existing ones in the literature. The physical and dynamical properties of the shell are as follows: E=200 GPa, ρ=7.8 g⁄cm^3 and w_{max} /H =1.

3.2 Numerical results of nonlinear frequencies

At first, material properties of sandwich microshell are listed in Table 3. As mentioned before, composite materials of the core layer were constituted by a mixture of graded GPLs and the Epoxy matrix, also the face layers made of epoxy. Beside the geometrical parameters of the GPLs are t_{GPL} = 2.5 nm, l_{GPL} = 2.5 μm, and b_{GPL} = 1.25 μm.

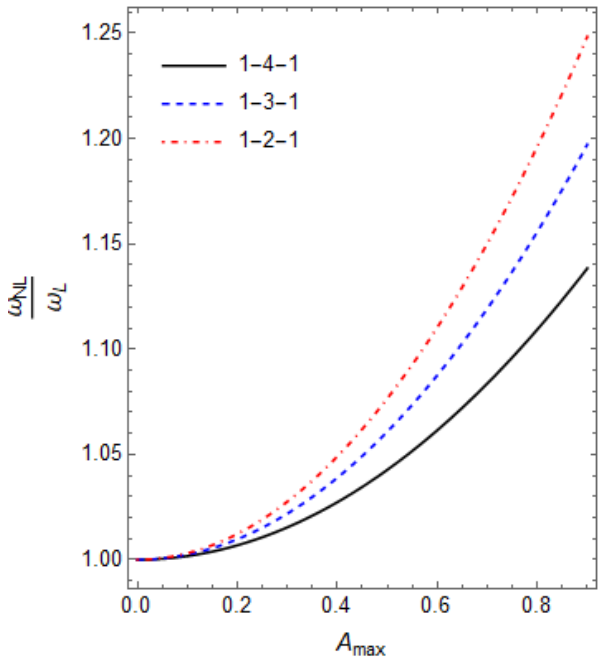

Fig. 3 Influence of the core to face thickness ratio on the first frequency and nonlinear backbone curve of sandwich micro shell in thermal environment

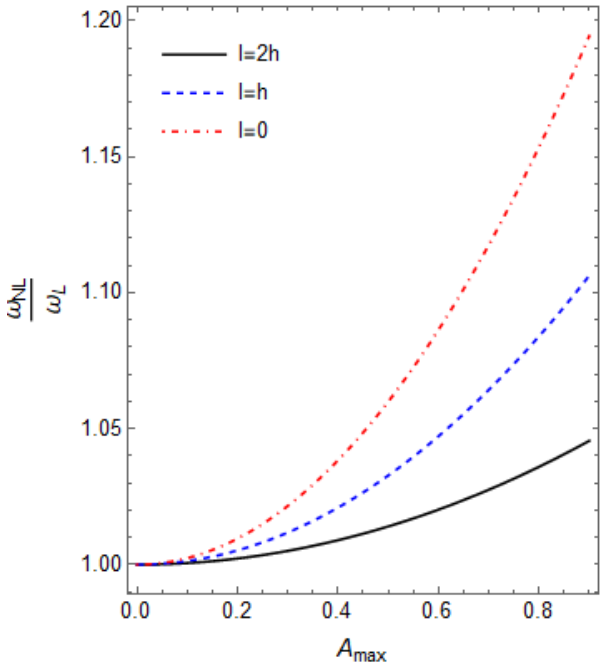

Fig. 4 Influence of the LS parameter on the first frequency and nonlinear backbone curve of sandwich micro shell in thermal environment

In this section, Influences of the sandwich microshell R/H, h/H and L/R ratios, material LS parameter (l), GPLs pattern and weight fraction (g_{GPL}), $(l/b)_{GPL}$, $(l/t)_{GPL}$ and temperature change of medium on the nonlinear-to-linear frequency ratios of the FG-GPL reinforced cylindrical microshell have been presented. In the numerical results study, If it was not specifically mentioned, the core layer has the GPL-A reinforced pattern with g_{GPL} = 0.4%.

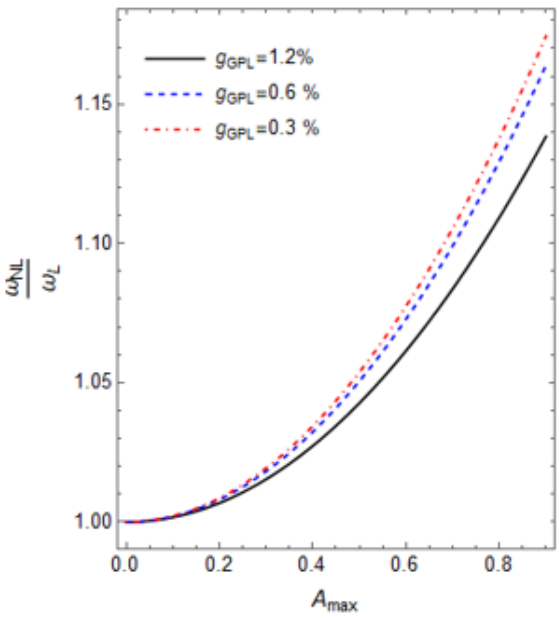

(a)

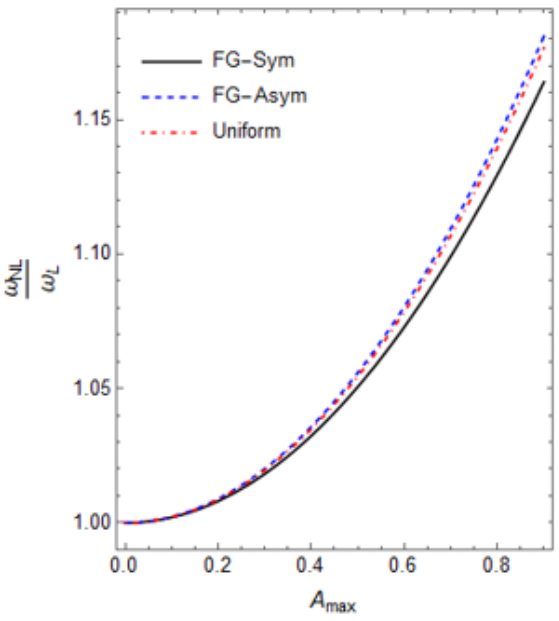

(b)

Fig. 5 The nonlinear backbone curve of the sandwich microshell with GPL- reinforced coer (a) at different weight fraction of GPLs, (b) at different GPLs patterns.

Fig. 3 illustrates the nonlinear to linear frequency ratio of a sandwich cylindrical shell with respect to core to total thickness ratio (configuration of sandwich shell). It is observed that increase in core to total thickness ratio (h/H) in a sandwich cylindrical panel enhances the structure stiffness value irrespective of GPL pattern. It's worth mentioning that for 1-X-1 configuration, the core to total thickness ratio equals to: $\frac{h}{H} = \frac{X}{X+2}$.

The nonlinear backbone curve were illustrated in Fig. 4 for different values of the LS parameter. Fig. 4 indicates that the hardening effect reduced as the LS parameter increased, since the linear stiffnesses of the microshell will increase by rising the l/h parameter (h remain unchanged). Considering the Fig. 4, it becomes evident that the LS parameter have a significant influence on the nonlinear response behavior of the structure, which is characterized by softening behavior. In other words, as observed from the diagrams, with an increase in the LS parameter, the nonlinear response curves bend towards the right, resulting in an increase in the shell's softening behavior. Conversely, as the LS parameter increase, the intensity of the microshell's hardening behavior decreases, and the diagram tilts towards the right. The reason for this behavior is that with an increase in the LS parameter, the strain energies of the shell material increases, leading to a increase in the overall stiffness of the shell, subsequently rising the natural frequency and softening behavior of the structure.

Influences of GPL weight fractions and GPL patterns on the nonlinear backbone curves for the sandwich cylindrical microshell have been shown in the Fig.5a and Fig. 5b, respectively. By increasing the parameter g_{GPL}, the hardening effect have been increased. Furthermore, it can be concluded that for a given the vibrational mode shape and circumferential and longitudinal wave numbers, increasing the value of GPL phase tends the nonlinear frequency response of the system to a softening behavior. According to the Fig.5b, the nonlinear-to-linear frequency ratios at FG-Sym pattern is the lowest among the three GPLs patterns. This phenomenon exposes that FG-Sym pattern can reach a better reinforcement effect arbitrating from the response of the resonance. It can be concluded that by existence of more GPL nearby inner and outer surfaces of the shell, the stiffness increased more.

The influence of the GPLs geometric size on the nonlinear-to-linear frequency ratios of the microshell have been shown in the Fig. 6 while the l_{GPL} remain unchanged. Based on the Fig. 6a, increasing of l_{GPL}/b_{GPL} value, leads to an increase in the nonlinear stiffness amplitude, due to reducing the surface area of GPLs (narrowing GPLs) will reduce the linear stiffness of the microshell, so the "hardening effect" became intense. As shown in the Figure 6b, the backbone curve rotates CCW with the increase of l_{GPL}/t_{GPL} value, due to reducing the thickness of GPLs and enhancing the "hardening effect" characteristics.

The influences of temperature rise of outher surface on the backbone curve of the sandwich shell with GPL reinforced core are illustrated in Fig. 7 when R/H=24 and L/R=12; and the circumferential wave number of fundamental modes equals to n=2. It can be seen that the temperature rise, increases the hardening effects, since the increase of temperature leads to reduction of the shell stiffness. Fig. 7 reveals the effect of temperature rise on frequency response of sandwich microshell in a thermal environment, while keeping the other parameters constant. The results of this diagram demonstrate that as the variations in ambient temperature increase, the first frequency of the system reduces. In fact, when the temperature of the outer surface increases, the thermal expansion coefficient of the material causes the shell to expand, which leads to an increase in its dimensions, and

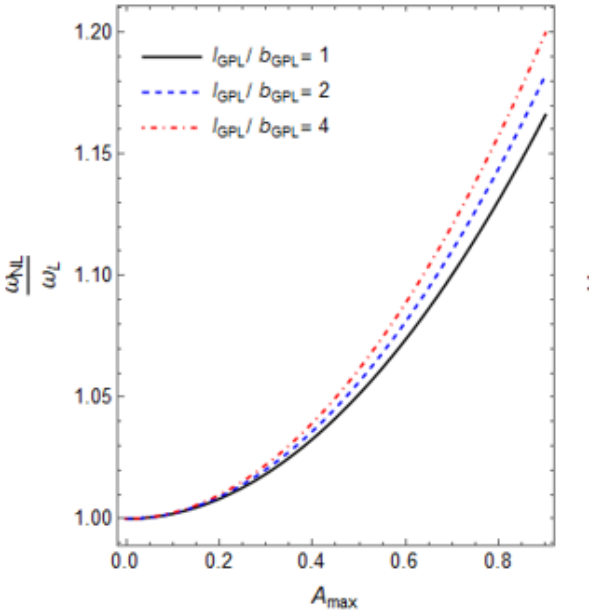

(a)

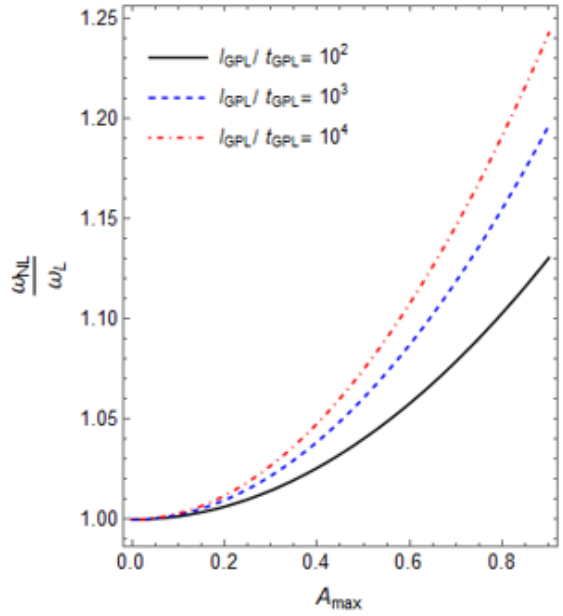

(b)

Fig. 6 The influence of the GPLs geometric size on the nonlinear backbone curve of the microshell with GPL-reinforced core (a) l_{GPL}/b_{GPL} ratio, (b) l_{GPL}/t_{GPL} ratio

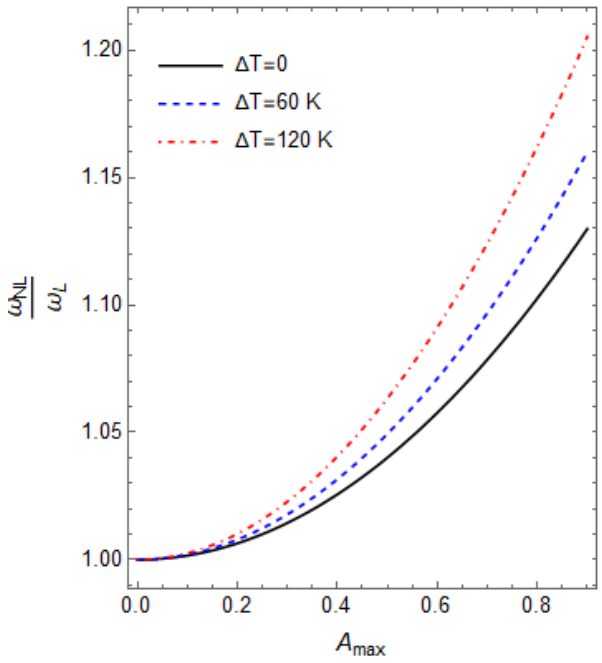

Fig. 7 The backbone curves of the microshell at different value of temperature rise of outer layer

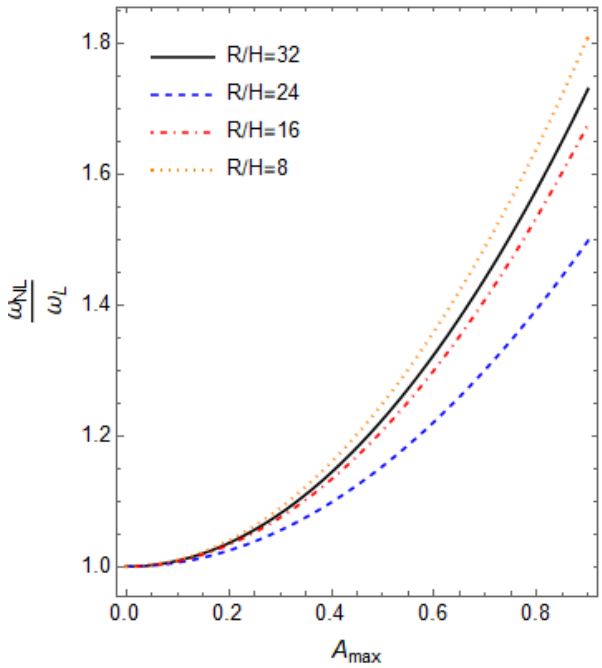

Fig. 8 Nonlinear-to-linear frequency ratio versus the max. vibration amplitude, for different R/H ratios

then results in a decrease in the stiffness of the shell, since the material becomes less resistant to deformation. As a result, the natural frequency of the shell decreases. This effect is more pronounced when the temperature change is significant or when the material has a high coefficient of thermal expansion.

Fig. 8 demonstrate the effects of the cylindrical shell radius to thickness (R/H) ratio on the backbone curves of nonlinear free vibration of the cylindrical shell when L/R=8. It can be concluded that by growing the R/H ratio, if the circumferential wave number of fundamental mode remain unchanged, hardening effects decreased; but if the circumferential wave number of fundamental mode changed, the hardening effects increased. For example, the circumferential wave number related to the fundamental mode of cylindrical shell change from n=3 to n=4, by increasing the ratio from R/H=24 to R/H=32.

The decrease in the hardening behavior and first frequency of sandwich shell, resulting from a lower R/H ratio, can be attributed to the higher bending stiffness of the shell associated with this ratio. This increased bending

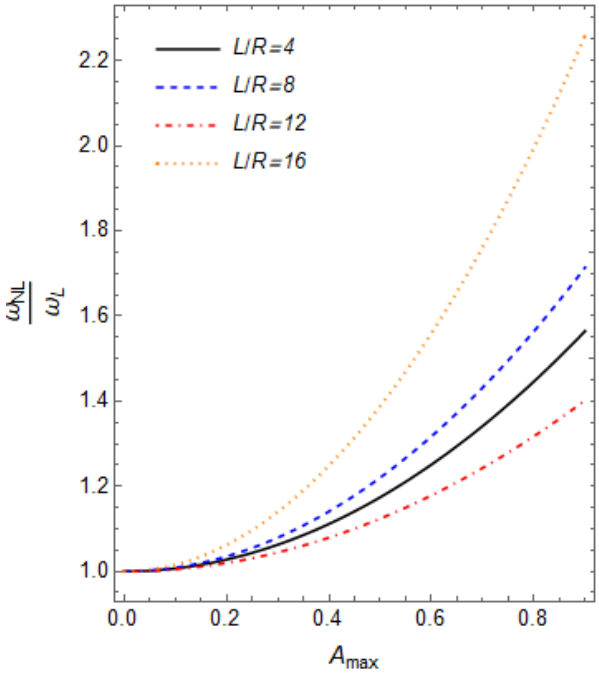

Fig. 9 The backbone curves for different value of L/R ratio of cylindrical sandwich microshell

stiffness enables the shell to resist deformation and displacement more effectively, resulting in a higher natural frequency and hardening behavior. Additionally, a lower R/H ratio also increases the radial stress in the shell, which further contributes to its increased stiffness. Consequently, the general outcome of decreasing the R/H ratio of a shell is a structure that is more rigid and stable, characterized by a higher natural frequency.

The effects of length-to-radius ratio (L/R) on the backbone curves of nonlinear frequencies for cylindrical microshell with R/H=30 are investigated in Fig. 9. The results indicate that by the increasing of L/R ratio from 8 to 12, the circumferential wave number changes from n=3 to n=2, then the hardening effects decreased. Hence, it can be initiate that when the circumferential and longitudinal wave numbers stay constant, the rising of the L/R ratio leads to increase the hardening effects, but in some cases which by increasing the L/R, the fundamental vibration mode shape and the circumference wave number are changed, the hardening effects decreased.

4. Conclusions

The present study investigated the size-dependent characteristics of free vibration for cylindrical sandwich microshells made by GPL-reinforced core in the presence of the thermal effects. The formulation was derived based on the MSGT and FSDT of shells under nonlinear geometric assumptions by taking into account and initial stresses due to thermal environment. The Hamilton principle was employed to derive the equations of motion, then the Galerkin method solved them analytically to obtain the nonlinear frequencies. From this study, some conclusions can be made:

(i) The LS parameter increases the nonlinearity; the nonlinear hardening behavior due to geometric nonlinearities increase in smaller l/h ratio microshell as the structural model becomes stiffer, reducing the impact of geometric nonlinearities.

(ii) Increasing the GPL to the polymeric matrix, specially nearby inner and outer surfaces of the shell, increase the stiffness and reduce nonlinearity of the reinforced composite.

(iii) Rising the temperature, increased the nonlinear hardening features of the shell.

(iv) The effects of length-to-radius ratio (L/R) and radius-to- thickness ratio (R/H) on the nonlinear frequencies of the sandwich shells show that Increasing the L/R and R/H ratios lead to change in the circumferential wave numbers of fundamental mode. However, the spring-hardening effect can decrease or increase by increasing the L/R and R/H ratios. It can be detected that when the circumferential wave numbers, and vibrational mode shape stay unchanged, the increase of the L/R and R/H ratios results in the hardening effects. However, by decreasing the L/R and R/H ratios, and changing the dominant circumferential wave number and vibration mode shape, a reverse behavior happens.

References

Abdollahi, R., Firouz-abadi, R.D. and Rahmanian, M. (2022), "Nonlinear vibrations and stability of rotating cylindrical shells conveying annular fluid medium", *Thin Walled Struct.*, **171**. https://doi.org/10.1016/j.tws.2021.108714.

Abo-Dahab, S.M., Abouelregal, A.E. and Marin, M. (2020), "Generalized thermoelastic functionally graded on a thin slim strip non-gaussian laser beam", *Symmetry*, **12**(7), 1094. https://doi.org/10.3390/sym12071094.

Alnujaie, A., Daikh, A.A., Ghazwani, M.H., Assie, A.E. and Eltaher, M.A. (2024), "Size-dependent free vibration of coated functionally graded graphene reinforced nanoplates rested on viscoelastic medium", *Adv. Nano Res.*, **17**(2), 181-195. https://doi.org/10.12989/anr.2024.17.2.181.

Ameer, S.A., Abdul Hussein, A.H., Mahdi, M.H., Elsaid, F.G. and Tahouneh, V. (2024), "Free vibration analysis of trapezoidal Double Layered plates embedded with viscoelastic medium for general boundary conditions using differential quadrature method", *Steel Compos. Struct.*, **50**(4), 429-441. https://doi.org/10.12989/scs.2024.50.4.429.

Anvari, M., Mohammadimehr, M. and Amiri, A. (2020), "Vibration behavior of a micro cylindrical sandwich panel reinforced by graphene platelet", *J. Vib. Control*, **26**(13-14). https://doi.org/10.1177/1077546319892730.

Barati, M.R. and Zenkour, A.M. (2019), "Vibration analysis of functionally graded graphene platelet reinforced cylindrical shells with different porosity distributions", *Mech. Adv. Mater. Struct.*, **26**(18), 1580-1588. https://doi.org/10.1080/15376494.2018.1444235.

Beni, Y.T., Mehralian, F. and Razavi, H. (2015), "Free vibration analysis of size-dependent shear deformable functionally graded cylindrical shell on the basis of modified couple stress theory", *Compos. Struct.*, **120**, 65-78. https://doi.org/10.1016/j.compstruct.2014.09.065.

Bhatti, M.M., Marin, M., Ellahi, R., Fudulu, I.M. (2023), "Insight into the dynamics of EMHD hybrid nanofluid (ZnO/CuO-SA) flow through a pipe for geothermal energy applications", *J.*

Therm. Anal. Calorim., **148**(96), 14261-14273. https://doi.org/10.1007/s10973-023-12565-8.

Bich, D.H. and Nguyen, N.X. (2012), "Nonlinear vibration of functionally graded circular cylindrical shells based on improved Donnell equations", *J. Sound Vib.*, **331**(25), 5488-5501. https://doi.org/10.1016/j.jsv.2012.07.024.

Bidzard, A., Malekzadeh, P. and Mohebpour, S.R. (2022), "A size-dependent nonlinear finite element free vibration analysis of multilayer FG-GPLRC toroidal micropanels in thermal environment", *Compos. Struct.*, **279**. https://doi.org/10.1016/j.compstruct.2021.114783.

Bouafia, H., Chikh, A., Bousahla,A.A., Bourada, F., Heireche, H., Tounsi, A., Benrahou, K.H., Tounsi,A., Al-Zahrani, M.M. and Hussain, M. (2021), "Natural frequencies of FGM nanoplates embedded in an elastic medium", *Adv. Nano Res.*, **11**(3), 239-249. https://doi.org/10.12989/anr.2021.11.3.239.

Boutaleb, S., Benrahou, K.H., Bakora, A., Algarni, A., Bousahla, A.A., Tounsi, A., Tounsi, A. and Mahmoud, S.R. (2019), "Dynamic analysis of nanosize FG rectangular plates based on simple nonlocal quasi 3D HSDT", *Adv. Nano Res.*, **7**(3), 191-208. https://doi.org/10.12989/anr.2019.7.3.191.

Chu, C., Al-Furjan, M.S.H. and Kolahchi, R. (2023), "Energy harvesting and dynamic response of SMA nano conical panels with nanocomposite piezoelectric patch under moving load", *Eng. Struct.*, **292**. https://doi.org/10.1016/j.engstruct.2023.116538.

Chu, C., Shan, L., Al-Furjan, M.S.H., Farrokhian, A. and Kolahchi, R. (2023), "Energy absorption, free and forced vibrations of flexoelectric nanocomposite magnetostrictive sandwich nanoplates with single sinusoidal edge on the frictional torsional viscoelastic medium", *Arch. Civil Mech. Eng.*, **23**. https://doi.org/10.1007/s43452-023-00756-x.

Chu, C., Shan, L., Al-Furjan, M.S.H., Zarei, M.S., Hajmohammad, M.H. and Kolahchi, R. (2022), "Experimental study for the effect of hole notched in fracture mechanics of GLARE and GFRP composites subjected to quasi-static loading", *Theor. Appl. Fract. Mech.*, **122**. https://doi.org/10.1016/j.tafmec.2022.103624.

Dai, Z., Jiang, Z., Zhang, L. and Habibi, M. (2021), "Frequency characteristics and sensitivity analysis of a size-dependent laminated nanoshell", *Adv. Nano Res.*, **10**(2), 175-189. https://doi.org/10.12989/anr.2021.10.2.175.

Ding, H.X. and She, G.L. (2023), "Nonlinear primary resonance behavior of graphene platelet-reinforced metal foams conical shells under axial motion", *Nonlinear Dyn.*, **111**(15), 13723-13752. https://doi.org/10.1007/s11071-023-08564-x.

Dong, Y., Hu, H. and Wang, L. (2022), "A comprehensive study on the coupled multi-mode vibrations of cylindrical shells", *Mech. Syst. Signal Process.*, **169**, 1-25. https://doi.org/10.1016/j.ymssp.2021.108730.

Dong, Y.H., Li, Y.H., Chen, D. and Yang, J. (2018), "Vibration characteristics of functionally graded graphene reinforced porous nanocomposite cylindrical shells with spinning motion", *Compos. Part B Eng.*, 145, 1-13. https://doi.org/10.1016/j.compositesb.2018.03.009.

Ebrahimi, F., Fardshad, R.E. and Mahesh, V. (2019), "Frequency response analysis of curved embedded magneto-electro-viscoelastic functionally graded nanobeams", *Adv. Nano Res.*, **7**(6), 391-403. https://doi.org/10.12989/anr.2019.7.6.391.

Gholami, R., Darvizeh, A., Ansari, R. and Sadeghi, F. (2016), "Vibration and buckling of first-order shear deformable circular cylindrical micro-/nano-shells based on Mindlin's strain gradient elasticity theory", *Eur. J. Mech.*, **58**, 76-88. https://doi.org/10.1016/j.euromechsol.2016.01.014.

Hasrati, E., Ansari, R. and Torabi, J. (2018), "A novel numerical solution strategy for solving nonlinear free and forced vibration problems of cylindrical shells", *App. Math. Modell.*, **53**, 653-672. https://doi.org/10.1016/j.apm.2017.08.027.

Hatami, S., Zarei, M.J. and Asghari Pari, S.H. (2024), "An innovative approach for analyzing free vibration in functionally graded carbon nanotube sandwich plates", *Adv. Nano Res.*, **17**(1), 19-32. https://doi.org/10.12989/anr.2024.17.1.019.

Hosseini-Hashemi, S., Abaei, A.R.R. and Ilkhani, M.R.R. (2015), "Free vibrations of functionally graded viscoelastic cylindrical panel under various boundary conditions", *Compos. Struct.*, **126**, 1-15. https://doi.org/10.1016/j.compstruct.2015.02.031.

Huang, X., Qi, X., Boey, F. and Zhang, H. (2012), "Graphene-based composites", *Chem. Soc. Rev.*, **41**(2), 666-686. https://doi.org/10.1039/C1CS15078B.

Jafari, A.A., Khalili, S.M.R. and Tavakolian, M. (2014), "Nonlinear vibration of functionally graded cylindrical shells embedded with a piezoelectric layer", *Thin Walled Struct.*, **79**, 8-15. https://doi.org/10.1016/j.tws.2014.01.030.

Khadir, A.I., Daikh, A.A. and Eltaher, M.A. (2021), "Novel four-unknowns quasi 3D theory for bending, buckling and free vibration of functionally graded carbon nanotubes reinforced composite laminated nanoplates", *Adv. Nano Res.*, **11**(6), 621-640. https://doi.org/10.12989/anr.2021.11.6.621.

Kim, H., Abdala, A., and Macosko, C. (2010), "Graphene/ polymer nanocomposites", *Macromolecules*, **43**(16), 6515-6530. https://doi.org/10.1021/ma100572e.

Liu, Z., Zhu, K., Wen, X. and Kumar, A. (2024), "Nonlinear vibration analysis of FG porous shear deformable cylindrical shells covered by CNTs-reinforced nanocomposite layers considering neutral surface exact position", *Adv. Nano Res.*, **17**(1), 61-73. https://doi.org/10.12989/anr.2024.17.1.061.

Ma, Z., Xing, B. and Liu, J. (2024), "Dynamic analysis of GPLs reinforced microcapsules subjected to moving micro/ nanoparticles using mathematical modeling and deep-neural networks", *Measurement*, **225**. https://doi.org/10.1016/j.measurement.2023.113940.

Marin, M. (2010), "Some estimates on vibrations in thermoelasticity of dipolar bodies", *J. Vib. Control*, **16**(1), 33-47. https://doi.org/10.1177/1077546309103419.

Marin, M., Seadawy, A. Vlase, S. and Chirila, A. (2022) "On mixed problem in thermoelasticity of type III for Cosserat media", *J. Taibah Univ. Sci.*, **16**(1), 1264-1274. https://doi.org/10.1080/16583655.2022.2160290.

Marin, M., Abbas, I. and Kumar, R. (2014), "Relaxed Saint-Venant principle for thermoelastic micropolar diffusion", *Struct. Eng. Mech.*, **51**(4), 651-662. https://doi.org/10.12989/sem.2014.51.4.651.

Mohammed, A.M., Mohammed, B.A., Kadhom, H.K., Taki, A.G. and Tahouneh, V. (2024), "A semi-analytical study for vibration analysis of damaged core laminated cylindrical shell with functionally graded CNTs reinforced face sheets resting on a two-parameter elastic foundation", *Adv. Nano Res.*, **17**(4), 301-313. https://doi.org/10.12989/anr.2024.17.4.301.

Niu, Y., Zhang, W. and Guo, X.Y. (2019), "Free vibration of rotating pretwisted functionally graded composite cylindrical panel reinforced with graphene platelets", *Eur. J. Mech. A Solids*, **77**. https://doi.org/10.1016/j.euromechsol.2019.103798.

Rafiee, M.A., Rafiee, J., Wang, Z., Song, H. and Koratkar, N. (2009), "Enhanced mechanical properties of nanocomposites at low graphene content", *ACS Nano*, **3**(12), 3884-3890. https://doi.org/10.1021/nn9010472.

Shen, H.S., Xiang, Y. and Fan, Y. (2017), "Nonlinear vibration of FG graphene-reinforced composite laminated cylindrical shells in thermal environments", *Compos. Struct.*, **182**, 447-456. https://doi.org/10.1016/j.compstruct.2017.09.010.

Shen, X., Li, T., Xu, L., Kiarasi, F., Babaei, M. and Asemi, K. (2024), "Free vibration analysis of FG porous spherical cap reinforced by graphene platelet resting on Winkler foundation", *Adv. Nano Res.*, **16**(1), 11-26.

https://doi.org/10.12989/anr.2024.16.1.011.
Soltanimaleki, A., Foroutan, M. and Alihemmati, J. (2016), "Free vibration analysis of functionally graded fiber reinforced cylindrical panels by a three dimensional mesh-free model", *J. Vib. Control*, **22**(19), 4087-4098. https://doi.org/10.1177/1077546315570717.
Tahouneh, V., Naei, M.H., Mosavi Mashhadi, M. (2019), "Using IGA and trimming approaches for vibrational analysis of L-shape graphene sheets via nonlocal elasticity theory", *Steel Compos. Struct.*, **33**(5), 717-727. https://doi.org/10.12989/scs.2019.33.5.717.
Tahouneh, V., Naei, M.H., Mosavi Mashhadi, M. (2020), "Influence of vacancy defects on vibration analysis of graphene sheets applying isogeometric method: Molecular and continuum approaches", *Steel Compos. Struct.*, **34**(2), 261-277. https://doi.org/10.12989/scs.2020.34.2.261.
Tohidi, H., Hosseini-Hashemi, S.H., Maghsoudpour, A. and Etemadi, S. (2017), "Dynamic stability of FG-CNTR viscoelastic micro cylindrical shells resting on orthotropic viscoelastic medium subjected to harmonic temperature distribution and magnetic field", *Wind Struct.*, **25**(2), 131-156. https://doi.org/10.12989/was.2017.25.2.131.
Tornabene, F. (2009), "Free vibration analysis of functionally graded conical cylindrical shell and annular plate structures with a four-parameter power-law distribution", *Comput. Meth. Appl. Mech. Eng.*, **198**(37), 2911-2935. https://doi.org/10.1016/j.cma.2009.04.011.
Tornabene, F. and Ceruti, A. (2013), "Mixed static and dynamic optimization of four-parameter functionally graded completely doubly curved and degenerate shells and panels using GDQ method", *Math. Probl. Eng.*, 1-33. https://doi.org/10.1155/2013/867079.
Tornabene, F., Bacciocchi, M., Fantuzzi, N. and Reddy, J.N. (2019), "Multiscale approach for three-phase cnt/polymer/fiber laminated nanocomposite structures", *Polym. Compos.*, **40**, 102-126. https://doi.org/10.1002/pc.24520.
Tornabene, F., Fantuzzi, N. and Bacciocchi, M. (2014), "Free vibrations of free-form doubly curved shells made of functionally graded materials using higher-order equivalent single layer theories", *Compos. Part B*, **67**(1), 490-509. https://doi.org/10.1016/j.compositesb.2014.08.012.
Veysi, A., Shabani, R. and Rezazadeh, G. (2017), "Nonlinear vibrations of micro-doubly curved shallow shells based on modified couple stress theory", *Nonlinear Dyn.*, **87**(3), 2051-2065. https://doi.org/10.1007/s11071-016-3175-5.
Wang, G., Zhu, Z., Zhang, Y., Xu, R., Jiang, Y. and Liu, Q. (2023), "Free and forced vibration analysis of thin-walled cylindrical shells with arbitrary boundaries in steady thermal environment", *Thin Walled Struct.*, **185**. https://doi.org/10.1016/j.tws.2023.110556.
Wang, Y.Q., Ye, C. and Zu, J.W. (2019), "Nonlinear vibration of metal foam cylindrical shells reinforced with graphene platelets", *Aerosp. Sci. Technol.*, **85**, 359-370. https://doi.org/10.1016/j.ast.2018.12.022.
Wu, C.P. and Liu, Y.C. (2016), "A state space meshless method for the 3D analysis of FGM axisymmetric circular plates", *Steel Compos. Struct.*, **22**(1), 161-182. https://doi.org/10.12989/scs.2016.22.1.161.
Wu, Z., Zhang, Y. and Yao, G. (2020), "Nonlinear forced vibration of functionally graded CNT reinforced composite circular cylindrical shells", *Acta Mech.*, **231**(6), 2497-2519. https://doi.org/10.1007/s00707-020-02650-6.
Yadav, A., Amabili, M., Panda, S.K., Dey, T., Kumar, R. (2021), "Forced nonlinear vibrations of cylindrical sandwich shells with cellular core using higher-order shear and thickness deformation theory", *J. Sound Vib.*, **510**, 1-22. https://doi.org/10.1016/j.jsv.2021.116283.
Yang, B., Yang, J. and Kitipornchai, S. (2017), "Thermoelastic analysis of FG graphene reinforced rectangular plates based on 3D elasticity", *Meccanica*, **52**(10), 2275-2292. https://doi.org/10.1007/s11012-016-0579-8.
Yadav, A.K., Carrera, E., Marin, M. and Othman M.I.A. (2024), "Reflection of hygrothermal waves in a Nonlocal Theory of coupled thermo-elasticity", *Mech. Adv. Mater. Struct.*, **31**(5), 1083-1096. https://doi.org/10.1080/15376494.2022.2130484.
Yin, B. and Fang, J. (2023), "Modified couple stress-based free vibration and dynamic response of rotating FG multilayer composite microplates reinforced with graphene platelets", *Arch. Appl. Mech.*, **93**(3), 1051-1079. https://doi.org/10.1007/s00419-022-02313-z.
Zahedinejad, P., Malekzadeh, P., Farid, M. and Karami, G. (2010), "A semi-analytical three-dimensional free vibration analysis of FG curved panels", *Int. J. Press. Vessel.*, **87**(8), 470-480. https://doi.org/10.1016/j.ijpvp.2010.06.001.

CC

Appendix A

$$C_{11} = \left(-\frac{A_{11}m^2\pi^3}{2L} - \frac{A_{66}Ln^2\pi}{2R^2} - \left(\frac{Ln^2\pi\mu_0 l^2}{2R^4} + \frac{Ln^4\pi\mu_0 l^2}{8R^4} + \frac{m^2n^2\pi^3\mu_0 l^2}{8LR^2}\right)\right);$$

$$C_{12} = \left(-\frac{A_{12}mn\pi^2}{2R} - \frac{A_{66}mn\pi^2}{2R} + \left(\frac{mn\pi^2\mu_0 l^2}{8R^3} + \frac{mn^3\pi^2\mu_0 l^2}{8R^3} + \frac{m^3n\pi^4\mu_0 l^2}{8L^2R}\right)\right);$$

$$C_{13} = \left(\frac{A_{12}m\pi^2}{2R} - \frac{mn^2\pi^2\mu_0 l^2}{4R^3}\right);$$

$$C_{14} = \left(-\frac{B_{11}m^2\pi^3}{2L} - \frac{B_{66}Ln^2\pi}{2R^2} - \left(-\frac{5Ln^2\pi\mu_0 l^2}{8R^3} + \frac{Ln^4\pi\mu_1 l^2}{8R^4} + \frac{m^2n^2\pi^3\mu_1 l^2}{8LR^2}\right)\right);$$

$$C_{15} = (-\frac{B_{12}mn\pi^2}{2R} - \frac{B_{66}mn\pi^2}{2R} - (\frac{mn\pi^2\mu_0 l^2}{8R^2} - \frac{mn\pi^2\mu_1 l^2}{4R^3} - \frac{mn^3\pi^2\mu_1 l^2}{8R^3} - \frac{m^3n\pi^4\mu_1 l^2}{8L^2R}));$$

$$C_{21} = \left(-\frac{A_{12}mn\pi^2}{2R} - \frac{A_{66}mn\pi^2}{2R} + \left(\frac{mn\pi^2\mu_0 l^2}{8R^3} + \frac{mn^3\pi^2\mu_0 l^2}{8R^3} + \frac{m^3n\pi^4\mu_0 l^2}{8L^2R}\right)\right);$$

$$C_{22} = \left(-\frac{A_{66}m^2\pi^3}{2L} - \frac{A_{22}Ln^2\pi}{2R^2} - \left(\frac{m^4\pi^5\mu_0 l^2}{8L^3} + \frac{Ln^2\pi\mu_0 l^2}{8R^4} + \frac{m^2\pi^3\mu_0 l^2}{4LR^2} + \frac{m^2n^2\pi^3\mu_0 l^2}{8LR^2}\right)\right);$$

$$C_{23} = \left(\frac{A_{22}Ln\pi}{2R^2} + \frac{E_{55}Ln\pi}{2R^2} + \left(\frac{Ln\pi\mu_0 l^2}{8R^4} + \frac{Ln^3\pi\mu_0 l^2}{8R^4} + \frac{3m^2n\pi^3\mu_0 l^2}{8LR^2}\right)\right);$$

$$C_{24} = \left(-\frac{B_{12}mn\pi^2}{2R} - \frac{B_{66}mn\pi^2}{2R} - \left(\frac{mn\pi^2\mu_0 l^2}{4R^2} + \frac{mn\pi^2\mu_1 l^2}{8R^3} - \frac{mn^3\pi^2\mu_1 l^2}{8R^3} - \frac{m^3n\pi^4\mu_1 l^2}{8L^2R}\right)\right);$$

$$C_{25} = (-\frac{B_{66}m^2\pi^3}{2L} - \frac{B_{22}Ln^2\pi}{2R^2} - (\frac{Ln^2\pi\mu_0 l^2}{8R^3} + \frac{3m^2\pi^3\mu_0 l^2}{8LR} + \frac{m^4\pi^5\mu_1 l^2}{8L^3} + \frac{m^2\pi^3\mu_1 l^2}{8LR^2} + \frac{m^2n^2\pi^3\mu_1 l^2}{8LR^2}));$$

$$C_{31} = \left(\frac{A_{21}m\pi^2}{2R} - \frac{mn^2\pi^2\mu_0 l^2}{4R^3}\right);$$

$$C_{32} = \left(\frac{A_{22}Ln\pi}{2R^2} + \frac{E_{55}Ln\pi}{2R^2} + \left(\frac{Ln\pi\mu_0 l^2}{8R^4} + \frac{Ln^3\pi\mu_0 l^2}{8R^4} + \frac{3m^2n\pi^3\mu_0 l^2}{8LR^2}\right)\right);$$

$$C_{33} = \left(-\frac{E_{44}m^2\pi^3}{2L} + \frac{m^2N_1^T\pi^3}{2L} - \frac{A_{22}L\pi}{2R^2} - \frac{E_{55}Ln^2\pi}{2R^2} + \frac{Ln^2N_2^T\pi}{2R^2} - \left(\frac{m^4\pi^5\mu_0 l^2}{8L^3} + \frac{Ln^2\pi\mu_0 l^2}{8R^4} + \frac{Ln^4\pi\mu_0 l^2}{8R^4} + \frac{m^2\pi^3\mu_0 l^2}{8LR^2} + \frac{m^2n^2\pi^3\mu_0 l^2}{4LR^2}\right)\right);$$

$$C_{34} = \left(-\frac{1}{2}E_{55}m\pi^2 + \frac{B_{21}m\pi^2}{2R} + \left(\frac{m^3\pi^4\mu_0 l^2}{8L^2} + \frac{m\pi^2\mu_0 l^2}{8R^2} + \frac{mn^2\pi^2\mu_0 l^2}{8R^2}\right)\right);$$

$$C_{35} = \left(\frac{B_{22}Ln\pi}{2R^2} - \frac{E_{55}Ln\pi}{2R} + \left(-\frac{Ln\pi\mu_0 l^2}{8R^3} + \frac{Ln^3\pi\mu_0 l^2}{8R^3} + \frac{m^2n\pi^3\mu_0 l^2}{8LR} + \frac{m^2n\pi^3\mu_1 l^2}{4LR^2}\right)\right);$$

$$C_{36} = \frac{1}{2}\left(-\frac{27A_{11}m^4\pi^5}{32L^3} - \frac{27A_{22}Ln^4\pi}{32R^4} - \frac{3A_{12}m^2n^2\pi^3}{32LR^2} - \frac{3A_{21}m^2n^2\pi^3}{32LR^2} - \frac{3A_{66}m^2n^2\pi^3}{8LR^2}\right);$$

$$C_{37} = \frac{1}{6}(-\frac{27A_{11}m^4\pi^5}{32L^3} - \frac{27A_{22}Ln^4\pi}{32R^4} - \frac{3A_{12}m^2n^2\pi^3}{32LR^2} - \frac{3A_{21}m^2n^2\pi^3}{32LR^2} - \frac{3A_{66}m^2n^2\pi^3}{8LR^2});$$

$$C_{41} = \left(-\frac{B_{11}m^2\pi^3}{2L} - \frac{B_{66}Ln^2\pi}{2R^2} - \left(-\frac{5Ln^2\pi\mu_0 l^2}{8R^3} + \frac{Ln^4\pi\mu_1 l^2}{8R^4} + \frac{m^2n^2\pi^3\mu_1 l^2}{8LR^2}\right)\right);$$

$$C_{42} = \left(-\frac{B_{12}mn\pi^2}{2R} - \frac{B_{66}mn\pi^2}{2R} - \left(\frac{mn\pi^2\mu_0 l^2}{4R^2} + \frac{mn\pi^2\mu_1 l^2}{8R^3} - \frac{mn^3\pi^2\mu_1 l^2}{8R^3} - \frac{m^3n\pi^4\mu_1 l^2}{8L^2R}\right)\right);$$

$$C_{43} = \left(-\frac{1}{2}E_{44}m\pi^2 + \frac{B_{12}m\pi^2}{2R} + \left(\frac{m^3\pi^4\mu_0 l^2}{8L^2} + \frac{m\pi^2\mu_0 l^2}{8R^2} + \frac{mn^2\pi^2\mu_0 l^2}{8R^2}\right)\right);$$

$$C_{44} = \left(-\frac{D_{11}m^2\pi^3}{2L} - \frac{D_{66}Ln^2\pi}{2R^2} - \left(\frac{m^2\pi^3\mu_0 l^2}{8L} + \frac{Ln^2\pi\mu_0 l^2}{2R^2} - \frac{Ln^2\pi\mu_1 l^2}{4R^3} + \frac{Ln^4\pi\mu_2 l^2}{8R^2} + \frac{m^2n^2\pi^3\mu_2 l^2}{8LR^2}\right)\right);$$

$$C_{45} = (-\frac{D_{12}mn\pi^2}{2R} - \frac{D_{66}mn\pi^2}{2R} + (\frac{3mn\pi^2\mu_0 l^2}{8R} - \frac{mn\pi^2\mu_1 l^2}{4R^2} + \frac{mn^3\pi^2\mu_2 l^2}{8R^3} + \frac{m^3n\pi^4\mu_2 l^2}{8L^2R}));$$

$$C_{51} = \left(-\frac{B_{21}mn\pi^2}{2R} - \frac{B_{66}mn\pi^2}{2R} + \left(-\frac{mn\pi^2\mu_0 l^2}{8R^2} + \frac{mn\pi^2\mu_1 l^2}{4R^3} + \frac{mn^3\pi^2\mu_1 l^2}{8R^3} + \frac{m^3n\pi^4\mu_1 l^2}{8L^2R}\right)\right);$$

$$C_{52} = \left(-\frac{B_{66}m^2\pi^3}{2L} - \frac{B_{22}Ln^2\pi}{2R^2} - \left(\frac{Ln^2\pi\mu_0 l^2}{8R^3} + \frac{3m^2\pi^3\mu_0 l^2}{8LR} + \frac{m^4\pi^5\mu_1 l^2}{8L^3} + \frac{m^2\pi^3\mu_1 l^2}{8LR^2} + \frac{m^2n^2\pi^3\mu_1 l^2}{8LR^2}\right)\right);$$

$$C_{53} = \left(\frac{B_{22}Ln\pi}{2R^2} - \frac{E_{55}Ln\pi}{2R} + \left(-\frac{Ln\pi\mu_0 l^2}{8R^3} + \frac{Ln^3\pi\mu_0 l^2}{8R^3} + \frac{m^2n\pi^3\mu_0 l^2}{8LR} + \frac{m^2n\pi^3\mu_1 l^2}{4LR^2}\right)\right);$$

$$C_{54} = \left(-\frac{D_{12}mn\pi^2}{2R} - \frac{D_{66}mn\pi^2}{2R} + \left(\frac{3mn\pi^2\mu_0 l^2}{8R} - \frac{mn\pi^2\mu_1 l^2}{4R^2} + \frac{mn^3\pi^2\mu_2 l^2}{8R^3} + \frac{m^3n\pi^4\mu_2 l^2}{8L^2R}\right)\right);$$

$$C_{55} = (-\frac{D_{66}m^2\pi^3}{2L} - \frac{D_{22}Ln^2\pi}{2R^2} - (\frac{m^2\pi^3\mu_0 l^2}{2L} + \frac{Ln^2\pi\mu_0 l^2}{8R^2} + \frac{m^2\pi^3\mu_1 l^2}{4LR} + \frac{m^4\pi^5\mu_2 l^2}{8L^3} + \frac{m^2\pi^3\mu_2 l^2}{4LR^2} + \frac{m^2n^2\pi^3\mu_2 l^2}{8LR^2}));$$

Appendix B

K_{iw} and K_{iww} ; (i = u, v, x, y) in Eq. (34) can be written as:

$$K_{uw}=\begin{bmatrix} C_{53}(-C_{12}C_{24}C_{45}+C_{12}C_{25}C_{44}+C_{14}C_{22}C_{45}-C_{14}C_{25}C_{42}-C_{15}C_{22}C_{44}+C_{15}C_{24}C_{42}) \\ +C_{43}(C_{12}C_{24}C_{55}-C_{12}C_{25}C_{54}-C_{14}C_{22}C_{55}+C_{14}C_{25}C_{52}+C_{15}C_{22}C_{54}-C_{15}C_{24}C_{52}) \\ +C_{23}(-C_{12}C_{44}C_{55}+C_{12}C_{45}C_{54}+C_{14}C_{42}C_{55}-C_{14}C_{45}C_{52}-C_{15}C_{42}C_{54}+C_{15}C_{44}C_{52}) \\ +C_{13}(C_{22}C_{44}C_{55}-C_{22}C_{45}C_{54}-C_{24}C_{42}C_{55}+C_{24}C_{45}C_{52}+C_{25}C_{42}C_{54}-C_{25}C_{44}C_{52}) \end{bmatrix}/\Delta C$$

$$K_{uww}=\begin{bmatrix} C_{56}(-C_{12}C_{24}C_{45}+C_{12}C_{25}C_{44}+C_{14}C_{22}C_{45}-C_{14}C_{25}C_{42}-C_{15}C_{22}C_{44}+C_{15}C_{24}C_{42}) \\ +C_{46}(C_{12}C_{24}C_{55}-C_{12}C_{25}C_{54}-C_{14}C_{22}C_{55}+C_{14}C_{25}C_{52}+C_{15}C_{22}C_{54}-C_{15}C_{24}C_{52}) \\ +C_{26}(-C_{12}C_{44}C_{55}+C_{12}C_{45}C_{54}+C_{14}C_{42}C_{55}-C_{14}C_{45}C_{52}-C_{15}C_{42}C_{54}+C_{15}C_{44}C_{52}) \\ +C_{16}(C_{22}C_{44}C_{55}-C_{22}C_{45}C_{54}-C_{24}C_{42}C_{55}+C_{24}C_{45}C_{52}+C_{25}C_{42}C_{54}-C_{25}C_{44}C_{52}) \end{bmatrix}/\Delta C$$

$$K_{vw}=\begin{bmatrix} C_{53}(C_{11}C_{24}C_{45}-C_{11}C_{25}C_{44}-C_{14}C_{21}C_{45}+C_{14}C_{25}C_{41}+C_{15}C_{21}C_{44}+C_{15}C_{24}C_{41}) \\ +C_{43}(-C_{11}C_{24}C_{55}+C_{11}C_{25}C_{54}+C_{14}C_{21}C_{55}-C_{14}C_{25}C_{51}-C_{15}C_{21}C_{54}+C_{15}C_{24}C_{51}) \\ +C_{23}(C_{11}C_{44}C_{55}-C_{11}C_{45}C_{54}-C_{14}C_{41}C_{55}+C_{14}C_{45}C_{51}+C_{15}C_{41}C_{54}-C_{15}C_{44}C_{51}) \\ +C_{13}(-C_{21}C_{44}C_{55}+C_{21}C_{45}C_{54}+C_{24}C_{41}C_{55}-C_{24}C_{45}C_{51}-C_{25}C_{41}C_{54}+C_{25}C_{44}C_{51}) \end{bmatrix}/\Delta C$$

$$K_{vww}=\begin{bmatrix} C_{56}(C_{11}C_{24}C_{45}-C_{11}C_{25}C_{44}-C_{14}C_{21}C_{45}+C_{14}C_{25}C_{41}+C_{15}C_{21}C_{44}-C_{15}C_{24}C_{41}) \\ +C_{46}(-C_{11}C_{24}C_{55}+C_{11}C_{25}C_{54}+C_{14}C_{21}C_{55}-C_{14}C_{25}C_{51}-C_{15}C_{21}C_{54}+C_{15}C_{24}C_{51}) \\ +C_{26}(C_{11}C_{44}C_{55}-C_{11}C_{45}C_{54}-C_{14}C_{41}C_{55}+C_{14}C_{45}C_{51}+C_{15}C_{41}C_{54}-C_{15}C_{44}C_{51}) \\ +C_{16}(-C_{21}C_{44}C_{55}+C_{21}C_{45}C_{54}+C_{24}C_{41}C_{55}-C_{24}C_{45}C_{51}-C_{25}C_{41}C_{54}+C_{25}C_{44}C_{51}) \end{bmatrix}/\Delta C$$

$$K_{xw}=\begin{bmatrix} C_{53}(-C_{11}C_{22}C_{45}+C_{11}C_{25}C_{42}+C_{12}C_{21}C_{45}-C_{12}C_{25}C_{41}-C_{15}C_{21}C_{42}+C_{15}C_{22}C_{41}) \\ +C_{43}(C_{11}C_{22}C_{55}-C_{11}C_{25}C_{52}-C_{12}C_{21}C_{55}+C_{12}C_{25}C_{51}+C_{15}C_{21}C_{52}-C_{15}C_{22}C_{51}) \\ +C_{23}(-C_{11}C_{42}C_{55}+C_{11}C_{45}C_{52}+C_{12}C_{41}C_{55}-C_{12}C_{45}C_{51}-C_{15}C_{41}C_{52}+C_{15}C_{42}C_{51}) \\ +C_{13}(C_{21}C_{42}C_{55}-C_{21}C_{45}C_{52}-C_{22}C_{41}C_{55}+C_{22}C_{45}C_{51}+C_{25}C_{41}C_{54}-C_{25}C_{42}C_{51}) \end{bmatrix}/\Delta C$$

$$K_{xww}=\begin{bmatrix} C_{56}(-C_{11}C_{22}C_{45}+C_{11}C_{25}C_{42}+C_{12}C_{21}C_{45}-C_{12}C_{25}C_{41}-C_{15}C_{21}C_{42}+C_{15}C_{22}C_{41}) \\ +C_{46}(C_{11}C_{22}C_{55}-C_{11}C_{25}C_{52}-C_{12}C_{21}C_{55}+C_{12}C_{25}C_{51}+C_{15}C_{21}C_{52}-C_{15}C_{22}C_{51}) \\ +C_{26}(-C_{11}C_{42}C_{55}+C_{11}C_{45}C_{52}+C_{12}C_{41}C_{55}-C_{12}C_{45}C_{51}-C_{15}C_{41}C_{52}+C_{15}C_{42}C_{51}) \\ +C_{16}(C_{21}C_{42}C_{55}-C_{21}C_{45}C_{52}-C_{22}C_{41}C_{55}+C_{22}C_{45}C_{51}+C_{25}C_{41}C_{54}-C_{25}C_{42}C_{51}) \end{bmatrix}/\Delta C$$

$$K_{yw}=\begin{bmatrix} C_{53}(C_{11}C_{22}C_{44}-C_{11}C_{24}C_{42}-C_{12}C_{21}C_{44}+C_{12}C_{24}C_{41}+C_{14}C_{21}C_{42}-C_{14}C_{22}C_{41}) \\ +C_{43}(-C_{11}C_{22}C_{54}+C_{11}C_{24}C_{52}+C_{12}C_{21}C_{54}-C_{12}C_{24}C_{51}+C_{14}C_{21}C_{52}+C_{14}C_{22}C_{51}) \\ +C_{23}(C_{11}C_{42}C_{54}-C_{11}C_{44}C_{52}-C_{12}C_{41}C_{54}+C_{12}C_{44}C_{51}+C_{14}C_{41}C_{52}-C_{14}C_{42}C_{51}) \\ +C_{13}(-C_{21}C_{42}C_{54}+C_{21}C_{44}C_{52}+C_{22}C_{41}C_{54}-C_{22}C_{44}C_{51}-C_{24}C_{41}C_{52}+C_{24}C_{42}C_{51}) \end{bmatrix}/\Delta C$$

$$K_{yww}=\begin{bmatrix} C_{56}(C_{11}C_{22}C_{44}-C_{11}C_{24}C_{42}-C_{12}C_{21}C_{44}+C_{12}C_{24}C_{41}+C_{14}C_{21}C_{42}-C_{14}C_{22}C_{41}) \\ +C_{46}(-C_{11}C_{22}C_{54}+C_{11}C_{24}C_{52}+C_{12}C_{21}C_{54}-C_{12}C_{24}C_{51}+C_{14}C_{21}C_{52}+C_{14}C_{22}C_{51}) \\ +C_{26}\big((C_{11}C_{42}C_{54}-C_{11}C_{44}C_{52}-C_{12}C_{41}C_{54}+C_{12}C_{44}C_{51}+C_{14}C_{41}C_{52}-C_{14}C_{42}C_{51})\big) \\ +C_{16}(-C_{21}C_{42}C_{54}+C_{21}C_{44}C_{52}+C_{22}C_{41}C_{54}-C_{22}C_{44}C_{51}-C_{24}C_{41}C_{52}+C_{24}C_{42}C_{51}) \end{bmatrix}/\Delta C$$

$$\Delta C=\begin{bmatrix} C_{11}(C_{55}C_{22}C_{44}-C_{22}C_{45}C_{54}-C_{24}C_{42}C_{55}+C_{24}C_{45}C_{52}+C_{25}C_{42}C_{54}-C_{25}C_{44}C_{52}) \\ +C_{12}(-C_{55}C_{21}C_{44}+C_{21}C_{45}C_{54}+C_{24}C_{41}C_{55}-C_{24}C_{45}C_{51}-C_{25}C_{41}C_{54}+C_{25}C_{44}C_{51}) \\ +C_{14}(C_{55}C_{21}C_{42}-C_{21}C_{45}C_{52}-C_{22}C_{41}C_{55}+C_{22}C_{45}C_{51}+C_{25}C_{41}C_{52}-C_{25}C_{42}C_{51}) \\ +C_{15}(-C_{54}C_{21}C_{42}+C_{21}C_{44}C_{52}+C_{22}C_{41}C_{54}-C_{22}C_{44}C_{51}-C_{24}C_{41}C_{52}+C_{24}C_{42}C_{51}) \end{bmatrix}$$